

Physical properties and evolutionary state of the Lyman alpha emitting starburst galaxy IRAS 08339+6517

H. Otí-Floranes^{1,2,3}, J.M. Mas-Hesse², E. Jiménez-Bailón¹, D. Schaerer^{4,5}, M. Hayes^{6,5}, G. Östlin⁷, H. Atek⁸, and D. Kunth⁹

¹ Instituto de Astronomía, Universidad Nacional Autónoma de México, Apdo. Postal 106, Ensenada B. C. 22800, Mexico
e-mail: otih@astrofísica.unam.mx

² Centro de Astrobiología (CSIC-INTA), Departamento de Astrofísica, POB 78, E-28691 Villanueva de la Cañada, Spain
e-mail: mm@cab.inta-csic.es

³ Dpto. de Física Moderna, Facultad de Ciencias, Universidad de Cantabria, 39005 Santander, Spain

⁴ Observatoire de Genève, Université de Genève, 51 Ch. des Maillettes, 1290 Versoix, Switzerland

⁵ CNRS, Institut de Recherche en Astrophysique et Planétologie, 14 avenue Edouard Belin, F-31400 Toulouse, France

⁶ Université de Toulouse, UPS-OMP, IRAP, Toulouse, France

⁷ Department of Astronomy, Oskar Klein Centre, Stockholm University, SE - 106 91 Stockholm, Sweden

⁸ Laboratoire d'Astrophysique, École Polytechnique Fédérale de Lausanne (EPFL), Observatoire, CH-1290 Sauverny, Switzerland

⁹ Institut d'Astrophysique de Paris (UMR 7095: CNRS & UPMC), 98 bis Bd Arago, 75014 Paris, France

Received; accepted

ABSTRACT

Context. Though Ly α emission is one of the most used tracers of massive star formation at high redshift, it is strongly affected by neutral gas radiation transfer effects. A correct understanding of these effects is required to properly quantify the star formation rate along the history of the Universe.

Aims. We aim to parameterize the escape of Ly α photons as a function of the galaxy properties, in order to properly calibrate the Ly α luminosity as a tracer of star formation intensity at any age of the Universe.

Methods. We are embarked in a program to study the properties of the Ly α emission (spectral profile, spatial distribution, relation to Balmer lines intensity,...) in a number of starburst galaxies in the Local Universe. The study is based on HST spectroscopic and imaging observations at various wavelengths, X-ray data and ground-based spectroscopy, complemented with the use of evolutionary population synthesis models.

Results. We present here the results obtained for one of those sources, IRAS 08339+6517, a strong Ly α emitter in the Local Universe which is undergoing an intense episode of massive star formation. We have characterized the properties of the starburst, which transformed $1.4 \times 10^8 M_{\odot}$ of gas into stars around 5 – 6 Myr ago. The mechanical energy released by the central Super Stellar Cluster (SSC) located in the core of the starburst has created a cavity devoid of gas and dust around it, leaving a clean path through which the UV continuum of the SSC is observed, with almost no extinction. While the average extinction affecting the stellar continuum is significantly larger out of the cavity, with $E(B-V)=0.15$ in average, we have not found any evidence for regions with very large extinctions, which could be hiding some young, massive stars not contributing to the global UV continuum. The observed soft and hard X-ray emissions are consistent with this scenario, being originated by the interstellar medium heated by the release of mechanical energy in the first case, and by a large number of active High Mass X-ray Binaries (HMXBs) in the second. In addition to the central compact emission blob, we have identified a diffuse Ly α emission component smoothly distributed over the whole central area of IRAS 08339+6517. This diffuse emission is spatially decoupled from the UV continuum, the H α emission or the H α /H β ratio. Both locally and globally, the Ly α /H α ratio is lower than the Case B predictions, even after reddening correction, with an overall Ly α escape fraction of only 4%.

Conclusions. We conclude that in IRAS 08339+6517 the Ly α photons resonantly scattered by an outflowing shell of neutral gas are being smoothly redistributed over the whole central area of the galaxy. Their increased probability of being destroyed by dust would explain the low Ly α escape fraction measured. In any case, in the regions where the diffuse Ly α emission shows the largest Ly α /H α ratios, no additional sources of Ly α emission are required, like ionization by hot plasma as proposed for Haro 2, another galaxy in our sample. These results stress again the importance of a proper correction of scattering and transfer effects when using Ly α to derive the star formation rate in high-redshift galaxies.

Key words. Galaxies: starburst – Galaxies: star formation – Galaxies: ISM – Ultraviolet: galaxies – Cosmology: observations – Galaxies: individual: IRAS 08339+6517

1. Introduction

The Ly α emission is one of the most useful tracers of massive star formation in the early Universe, since at high redshift it becomes visible in the optical-infrared range. Moreover, for red-

shifts above $z \sim 4$ it becomes the only emission line easily accessible from ground-based telescopes. But the study of Ly α emission in starburst galaxies in the Local Universe has shown that radiation transfer through neutral hydrogen can completely distort its properties, affecting its profile and intensity, and even transforming the emission into a damped absorption when the column

Send offprint requests to: J.M. Mas-Hesse

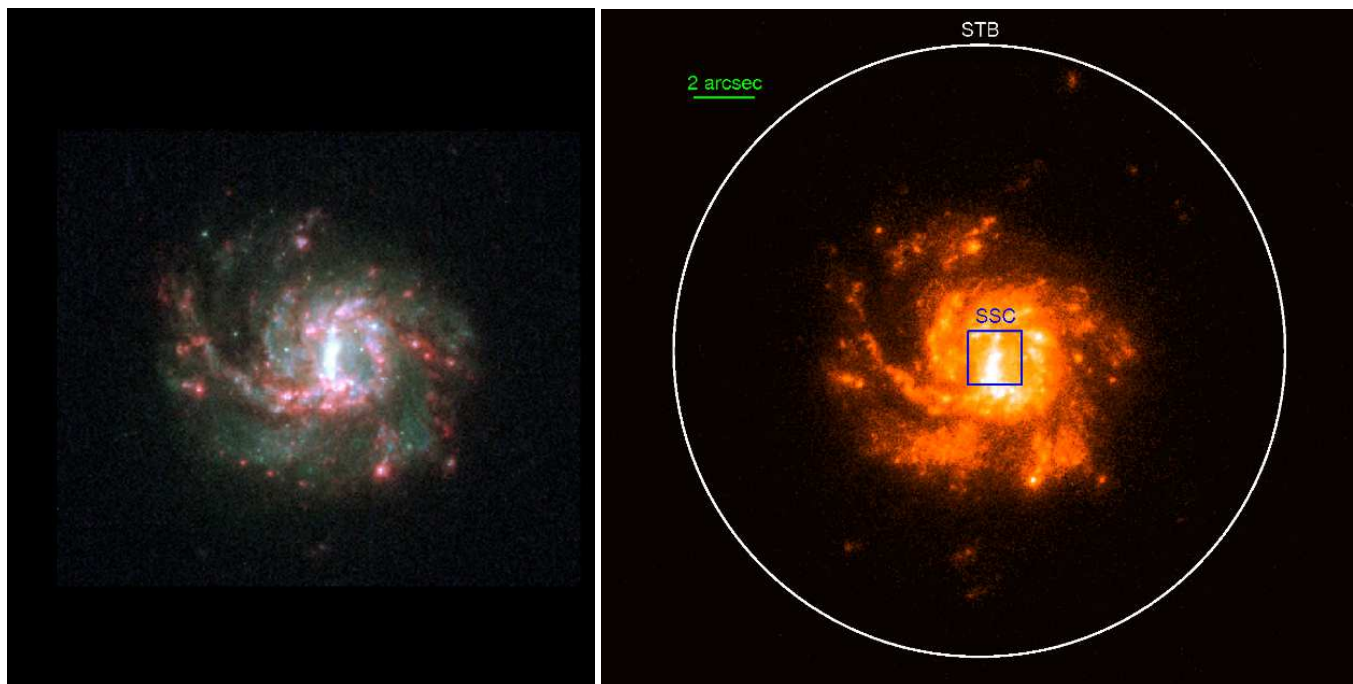


Fig. 1. **Left:** multispectral HST/ACS image of IRAS 0833. Blue: F300W, green: F435W, red: FR656N (Courtesy of Ángel R. López-Sánchez – AAO). **Right:** F140LP UV image. Integrated emission of the starburst (STB) and central Super Stellar Cluster (SSC) are labelled. Intensity scale is logarithmic. Same spatial scale in both images, as marked on the right panel. North is up and east is left.

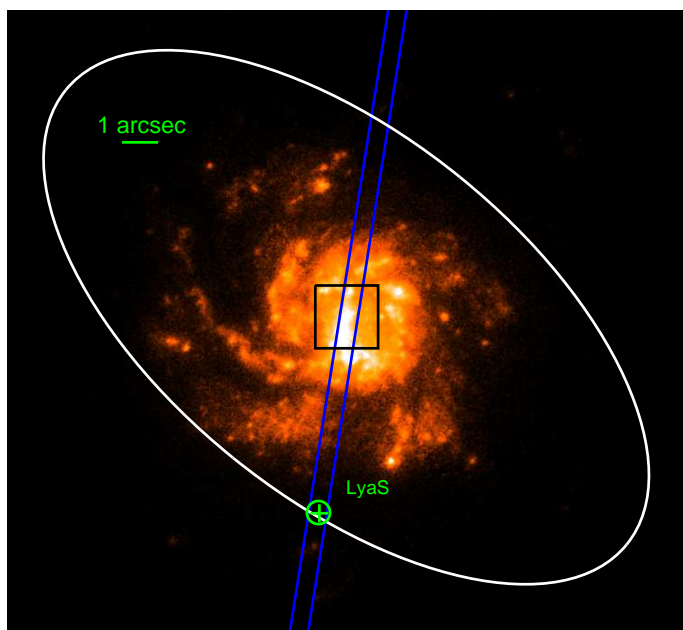


Fig. 2. F140LP UV image. HST/GHRS (squared) and IUE (oval) apertures are superimposed, together with the location of the STIS slit. The width of the apertures and the slit are represented at real scale. The location of the region Ly α S discussed in Sect. 4.3 is marked with a cross within a circle. Intensity scale is logarithmic. North is up and east is left.

density of neutral gas is high enough (Mas-Hesse et al. 2003). In order to investigate further the properties of the Ly α emission, and its correlation with other characteristics of the starbursts originating it, we are embarked in a program to study in detail Ly α emitting galaxies in the Local Universe (Östlin et al. 2009; Otf-Floranés et al. 2012; Hayes et al. 2013a). The final aim of this program is the proper calibration of Ly α as a tracer of star

formation, which could be used to derive the star formation intensity along the history of the Universe. In this work we present a detailed multiwavelength analysis of the Ly α emitting galaxy IRAS 08339+6517, complementing previous partial results by Mas-Hesse et al. (2003) and Östlin et al. (2009).

IRAS 08339+6517 (hereinafter IRAS 0833) is a face-on spiral galaxy at 80.2 Mpc, which is undergoing a starburst episode and shows a prominent Ly α emission line. The brightest UV knots are aligned along an internal bar oriented close to the *N*–*S* direction (Östlin et al. 2009). López-Sánchez et al. (2006) derived an age of 4 – 6 Myr for the most recent burst using H α spectroscopic data. They also estimated that there exist two older underlying stellar populations with ages 100 – 200 Myr and 1 – 2 Gyr. Cannon et al. (2004) reported from NRAO VLA data that IRAS 0833 harbours $1.1 \times 10^9 M_{\odot}$ of neutral hydrogen. They also detected a tidal stream between IRAS 0833 and its minor companion 2MASX J08380769+6508579, estimating for the stream material a mass of $3.8 \times 10^9 M_{\odot}$. The Ly α emission of IRAS 0833 was first reported by Kunth et al. (1997) from the analysis of HST/GHRS high-resolution spectrum of its nuclear region. They found that the Ly α line shows a P Cyg profile, as well as the presence of a blueshifted secondary Ly α emission component, on top of the spectral P Cyg trough. From the same data, Kunth et al. (1998) measured the flux of the line, as well as the column density of the neutral hydrogen which produces the observed P Cyg absorption. Later, HST/STIS long-slit observations with high spectral resolution led Mas-Hesse et al. (2003) to confirm that Ly α photons can actually escape from IRAS 0833 because most of the neutral gas surrounding the source is being pushed out by the starburst activity. The velocity shift causes that, whereas the blue photons of the line are actually resonantly scattered by H I, the red wing eventually escapes, leading to the observed P Cyg profile. They measured the velocity of expansion of the superbubble deriving $\sim 300 \text{ km s}^{-1}$. They argued that the secondary Ly α emission could be produced at the leading

front of the superbubble with no neutral hydrogen ahead, explaining why this minor component is detected blueshifted by $\sim 300 \text{ km s}^{-1}$ on top of the absorption trough caused by the out-flowing medium. Table 1 summarizes the basic properties of the starburst galaxy IRAS 0833.

In this work we have analyzed HST, XMM-Newton, IUE and ground-based observations aiming to characterize the properties of the starburst in IRAS 0833, and in order to check whether the conclusions from the study of Haro 2 (also known as Mrk 33 and IRAS 10293+5439) by Otí-Flóranes et al. (2012) about the nature of the diffuse, extended Ly α emission, could be extended to another Ly α emitting starburst galaxy with very different morphology and global properties. We describe the observational data in Sect. 2, the results are presented in Sect. 3, and they are discussed in Sect. 4. Finally, conclusions are outlined in Sect. 5.

2. Observational data and synthesis models

2.1. HST observations: ultraviolet and optical

We have used HST observations of IRAS 0833 obtained with ACS, STIS and GHRS, in the UV and optical. In this section we describe the data and the processing done.

2.1.1. HST images

The UV, optical and H α images used in this work were obtained and processed by Östlin et al. (2009) from HST/ACS observations. The UV image we will use to study the distribution of the massive, young stellar clusters corresponds to the observation with the F140LP filter (PI: Kunth). On the other hand, the H α image was created from the observation with the narrow filter FR656N, estimating the H α continuum by fitting pixel by pixel UV-optical photometric data points (HST/ACS F140LP, F220W, F330W, F435W and F550M observations) with SED's obtained from Starburst99 synthesis models (Leitherer et al. 1999). The resulting continuum was subtracted from the FR656N image. For a more complete description of the methodology, see Östlin et al. (2009). We show in Fig. 1 (left panel) a multispectral image created by Ángel R. López-Sánchez (CSIRO/ATNF) combining the HST/ACS images obtained with the F300W, F435W and FR656N filters. In the right panel, the regions which we will analyze in the paper are labelled on top of the F140LP image: 1) the spatially integrated emission, which comprises the total radiation from the whole starburst in IRAS 0833 (STB), and 2) the central supermassive stellar cluster (SSC).

2.1.2. HST spectroscopy

We have reanalyzed in this work the low-resolution GHRS spectroscopic data of IRAS 0833 described by González Delgado et al. (1998) as well as the high resolution, long-slit HST/STIS observations obtained by Mas-Hesse et al. (2003). Previous high resolution HST/GHRS observations by Kunth et al. (1998) were not used, since the HST/STIS data provided a broader wavelength coverage and higher spatial resolution along the long slit. The GHRS observation was performed with a squared aperture $1.7'' \times 1.7''$ centered on the maximum of the UV emission of IRAS 0833, i.e. its nucleus. Given its limited size, the aperture covered only the region around the central supermassive stellar cluster (SSC). The spectral coverage of the spectrum was 1100 – 1900 Å, which thus includes the Ly α line as well as the stellar absorption lines

Si IV $\lambda\lambda 1394, 1403 \text{ Å}$ and C IV $\lambda\lambda 1548, 1551 \text{ Å}$. The log of the HST/GHRS observations is shown in Table 2.

The G140M and G430L gratings were used in the STIS observations of the source. A $52'' \times 0.5''$ slit was placed onto the nucleus of IRAS 0833 with a position angle of 171° . High spectral resolution data of the Ly α line and the UV continuum in the spectral range 1200 – 1250 Å were obtained with G140M. The G430L spectral image includes the emission of the nebular lines O [II]3727, H β and O [III]4959, 5007. However, the integration time for G430L was very low, and the observation was severely affected by cosmic rays. The extraction and background removal processes in the STIS spectral images were carried out using IRAF¹, following the procedure described by Otí-Flóranes et al. (2012) for the STIS observation along the minor axis of the starburst galaxy Haro 2. See Mas-Hesse et al. (2003) for a more detailed description. The observation journal is included in Table 3. Figure 2 illustrates the position of the GHRS aperture and the STIS slit onto the ACS F140LP UV image of IRAS 0833.

2.2. IUE observations

The IUE/SWP and LWP spectra of IRAS 0833 were downloaded from the IUE Newly Extracted Spectra (INES) archive at CAB (Centre of Astrobiology, Madrid, <http://sdc.cab.inta-csic.es/ines/>). They were obtained with the IUE large aperture ($20'' \times 10''$), which enclosed most of the UV emission of the source. The spectral coverage of the cameras are 1150 – 1980 Å (SWP) and 1850 – 3350 Å (LWP). In Fig. 2 the position of its Large Aperture relative to the ACS F140LP UV image of IRAS 0833 is shown. The log of the IUE observation is shown in Table 2.

2.3. XMM-Newton: X-rays

XMM-Newton observation 0111400101 of π^1 Ursae Majoris (PI: Albert Brinkman) included IRAS 0833 in its field of view $\sim 8'$ away from the optical axis. Data from XMM-Newton analyzed in this work were obtained by the European Photon Imaging Camera (EPIC), which consists of 2 MOS (Metal Oxide Semi-conductor) and 1 pn CCD arrays. Each detector is located in a different X-ray telescope on-board XMM-Newton, and whereas only around half of the radiation entering the corresponding telescopes reaches the MOS cameras, the pn camera receives an unobstructed beam. The EPIC observation consisted in imaging of the source with Full Frame (MOS1) and Small Window (MOS2), as well as one timing observation (pn). We focused on the MOS1 and MOS2 imaging observations since we are not interested in the timing analysis of the source. Total exposure time of the observation was 50.1 ks (MOS1) and 45.2 ks (MOS2). Reduction of the data was performed with the Scientific Analysis Software 13.0.0 (SAS), following the standard threads available in the website of the XMM-Newton-SAS. Only spectral range 0.3 – 10.0 keV was considered, as well as events with patterns² $PATTERN \leq 4$ in order to maximize the signal-to-noise ratio (SNR) against non-X-rays events. Source regions in the EPIC images were calculated with SAS

¹ IRAF is distributed by the National Optical Astronomy Observatory, which is operated by the Association of Universities for Research in Astronomy (AURA) under cooperative agreement with the National Science Foundation.

² PATTERN describes how the charge cloud released by the incoming X-ray photon distributes over the pixels. See the SAS manual for a more detailed description.

Table 1. IRAS 0833 coordinates, redshift, distance, scale, Galactic H I, color excess toward the source, and oxygen abundance.

R. A. (J2000.0)	Decl. (J2000.0)	Redshift ^a	Distance ^a (Mpc)	Scale ^a (pc arcsec ⁻¹)	$N(\text{H I})_{\text{Gal}}^b$ (cm ⁻²)	$E(B-V)_{\text{Gal}}$	$12 + \log(\text{O/H})^c$
08 38 23.18	+65 07 15.20	0.0191	80.2	390	4.5×10^{20}	0.094	8.45

^a From NED (the NASA/IPAC Extragalactic Database).^b Average value from Dickey & Lockman (1990) and Kalberla et al. (2005).^c Value from López-Sánchez et al. (2006).**Table 2.** Log of HST/GHRS and IUE observations of IRAS 0833 used in this work.

Instrument	PI	Observation date	Grating/Camera	Integration time (s)	Aperture size	Position angle (deg)	Wavelength interval (Å)	Spectral dispersion (Å pixel ⁻¹)
HST/GHRS	Robert	1995 Dec 31	G140L	18088	1.7'' × 1.7''	-	1100 – 1900	0.573
IUE	Thuan	1989 Feb 13	SWP	4920	20'' × 10''	51	1150 – 1980	1.68
IUE	Thuan	1989 Feb 13	LWP	18000	20'' × 10''	51	1850 – 3350	2.67

Table 3. Log of HST/STIS observations of IRAS 0833 used in this work.

Observation date	PI	Grating	Detector	Integration time (s)	Position angle (deg)	Slit size	Wavelength interval (Å)	Plate scale (arcsec pixel ⁻¹)	Spectral dispersion (Å pixel ⁻¹)
2001 Jan 15	Kunth	G140M	MAMA	7320	171	52'' × 0.5''	1200 – 1250	0.029	0.053
2001 Jan 15	Kunth	G430L	CCD	360	171	52'' × 0.5''	2900 – 5700	0.050	2.746

task `eregionanalyse` in order to increase the SNR value over the background, resulting in circular regions with *radius* of 31'' (MOS1) and 28'' (MOS2). Redistribution matrices and ancillary files were calculated for the MOS1 and MOS2 images assuming the source regions for each image from which spectrum was extracted. Figure 3 shows the MOS1 and MOS2 images, together with the circular source regions assumed and the UV countours from the HST/ACS F140LP image. Source in MOS2 happened to be located close to a CCD border, and thus a fraction of the total X-ray emission may have been missed in this image. For consistency, when modeling the total spectrum we checked that similar results were obtained for both MOS spectra. Background was extracted from two circular regions with *radius* $\sim 1'$ with different locations in each of the two images but which would be close to IRAS 0833 and would not include any bright source. A net count rate of $\sim 1.5 \times 10^{-2}$ cts s⁻¹ was measured in the source regions after background subtraction. We used *XSPEC* v.12.8 (Arnaud 1996) to analyze the spectral data. Source counts were grouped to have at least 25 counts per bin in order to be able to apply χ^2 statistics in the fitting analysis. The final binned X-ray spectrum of IRAS 0833 is shown in Fig. 11. Since this is an off-axis observation, the point spread function (PSF) of the instrument is large and distorted. We compared the radial profiles of the source with the EPIC PSF using SAS task `eradial` at low, medium and high energy, and concluded that IRAS 0833 is not resolved and can be treated as a point-like source. Therefore, no information on the structure of the X-ray-emitting regions is available in Fig. 3, but just the spectral properties of their integrated emission.

2.4. Ground-based observations

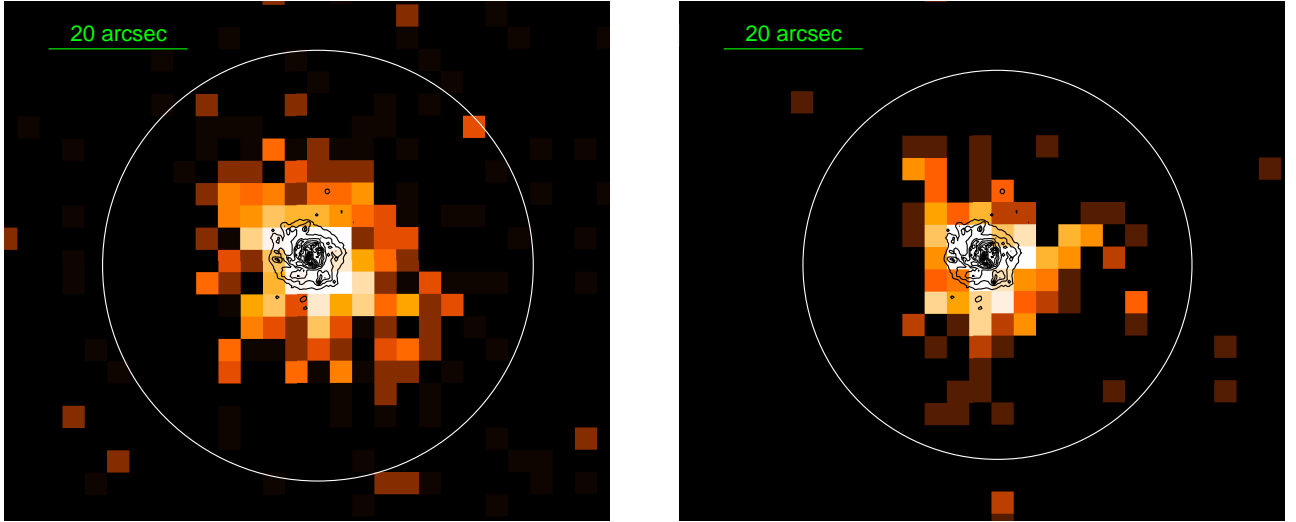
Two long-slit observations with the blue and red arms of William Herschel Telescope/ISIS were downloaded from the archive (PI: Ángel R. López-Sánchez). The location and position angle of the 1.0''-wide ISIS slit coincided with that of the HST/STIS slit. The spatial profiles of the H α and H β emission lines were extracted from the ISIS spectral images. The log of these observations is included in Table 4.

2.5. Synthesis models

Evolutionary population synthesis models by Leitherer et al. (1999) (Starburst 99, hereinafter SB99) and Cerviño et al. (2002) (hereinafter CMHK02) have been used to characterize the star formation episode taking place in IRAS 0833. Both sets of models compute the evolution of a cluster of massive stars for a given initial mass function, metallicity and star formation regime. Once the structure (number of stars of each spectral type and luminosity class at a given evolutionary time) of the stellar population is derived, the models are used to calculate a set of observable parameters (continuum emission, number of ionizing photons produced, supernova rate, equivalent width and intensity of nebular lines, etc.). Two different star formation regimes are considered in these models: 1) stars are produced at a constant rate (extended burst, EB), and 2) prompt formation occurs during a short period of time, after which no more stars are produced (instantaneous burst, IB). For consistency, we assume in both cases the same Salpeter initial mass function (IMF, $\phi(m) \sim m^{-2.35}$) with mass limits of 2 – 120 M $_{\odot}$. While the lower mass stars do not produce any observable effect in the UV range, they provide the bulk of the stellar mass and can even dominate the optical–IR continuum after some tens of Myr of evolution. The output magnitudes of the models are scaled by the intensity of star forma-

Table 4. Log of WHT/ISIS observations of IRAS 0833 used in this work.

Observation date	PI	Arm	Grating	Integration time (s)	Position angle (deg)	Slit size	Wavelength interval (Å)	Plate scale (arcsec pixel ⁻¹)	Spectral dispersion (Å pixel ⁻¹)
2006 Dec 25	López	Blue arm	R600B	3600	171	3.3' × 1.0''	3460 – 5280	0.20	0.45
2006 Dec 25	López	Red arm	R600R	3600	171	3.3' × 1.0''	5690 – 7745	0.22	0.49


Fig. 3. XMM-Newton/EPIC MOS1 (left) and MOS2 (right) X-ray images of IRAS 0833. Intensity scale is logarithmic. Source region from which X-ray spectrum was extracted for each camera is confined within the white circle. Contours from HST/ACS F144LP image are shown in black. PSF of this off-axis observation is large and asymmetric, and thus the emission must be considered as non-resolved. North is up and east is left.

tion, which is characterized by the star formation rate (SFR, the velocity at which stars are being produced) in EB models, and star formation strength (SFS, total mass converted into stars) in IB models. See the cited references for a more detailed description of the models.

3. Analysis and results

3.1. HST morphology and photometry

The F140LP UV image in Fig. 1 shows that IRAS 0833 is composed of a large, bright central stellar cluster along an internal bar almost aligned from N to S, surrounded by a rather diffuse UV emission from several spiral arms which enclose smaller, unresolved stellar knots. Whereas the elongated central cluster is comprised within $1'' \times 2''$ (~ 400 pc \times 800 pc), the spiral arms extend over a circular region of *radius* $\sim 5.5''$ (~ 2 kpc). As shown in the right panel of Fig. 1, hereinafter we will refer to the global starburst in IRAS 0833 as STB, and we will characterize it by analyzing the integrated emission of the whole source. On the other hand, we have labelled its central UV-bright stellar cluster as SSC, whose emission is roughly included within the GHRS aperture.

The observed total UV flux of the STB region (F_{1529}) was measured at 1500 Å rest frame in two ways: 1) through the integrated emission of HST/ACS F140LP image, and 2) from the flux at 1500(1 + z) Å in the IUE spectrum. Although very large, the IUE aperture might have not included the whole emission from the source. To check whether this was the case, we calculated both the total integrated flux from the HST/ACS F140LP image ($F_{UV}^{integrated}$), as well as the flux enclosed in the same image by an aperture similar to the IUE one positioned with the same angle (F_{UV}^{IUE}), as shown in Fig. 2. We derived a ratio

$F_{UV}^{integrated}/F_{UV}^{IUE} = 1.04$, indicating that the IUE aperture encloses 96% of the UV emission of IRAS 0833. After correcting for this aperture loss, the value of the IUE UV flux remains 15% lower than the integrated HST/ACS F140LP flux. The disagreement is most likely a combination of the 10% photometric accuracy of IUE (see Fig. 7) and the very broad, skewed shape of the F140LP filter. We therefore decided to take the average of both flux measurements as the total UV flux at 1500 Å of STB, $F_{1529} = 4.5 \times 10^{-14}$ erg s⁻¹ cm⁻² Å⁻¹. This uncertainty in the measurement of F_{1529} translates into a systematic uncertainty of $\pm 10\%$ in the determination of any absolute magnitude of STB based on it, like the total mass of the starburst or the predicted luminosities at different ranges.

Given the size of its aperture, the spectrum obtained by HST/GHRS includes mostly the emission from the central cluster, which we have labelled SSC. The UV flux value found for this region $F_{1529} = 8.5 \times 10^{-15}$ erg s⁻¹ cm⁻² Å⁻¹ is 20% of STB, i.e. the total integrated observed UV flux of IRAS 0833.

We show in Fig. 4 a color-coded image of IRAS 0833 combining F140LP UV (green) and H α (red), along with the single images of each filter, as generated by Östlin et al. (2009), and merged together using *ds9* (Joye & Mandel 2003). While in the H α image a filamentary structure extending largely around the stellar clusters in the spiral arms appears very prominent, the region dominated by the UV-bright SSC shows a very low H α emission, if any.

3.2. UV stellar continuum

In order to estimate the evolutionary state of the star formation episode in IRAS 0833, the profile of the spectral lines Si IV $\lambda\lambda 1394, 1403$ Å and C IV $\lambda\lambda 1548, 1551$ Å in the normalized HST/GHRS (SSC) and IUE (STB) spectra were fitted using

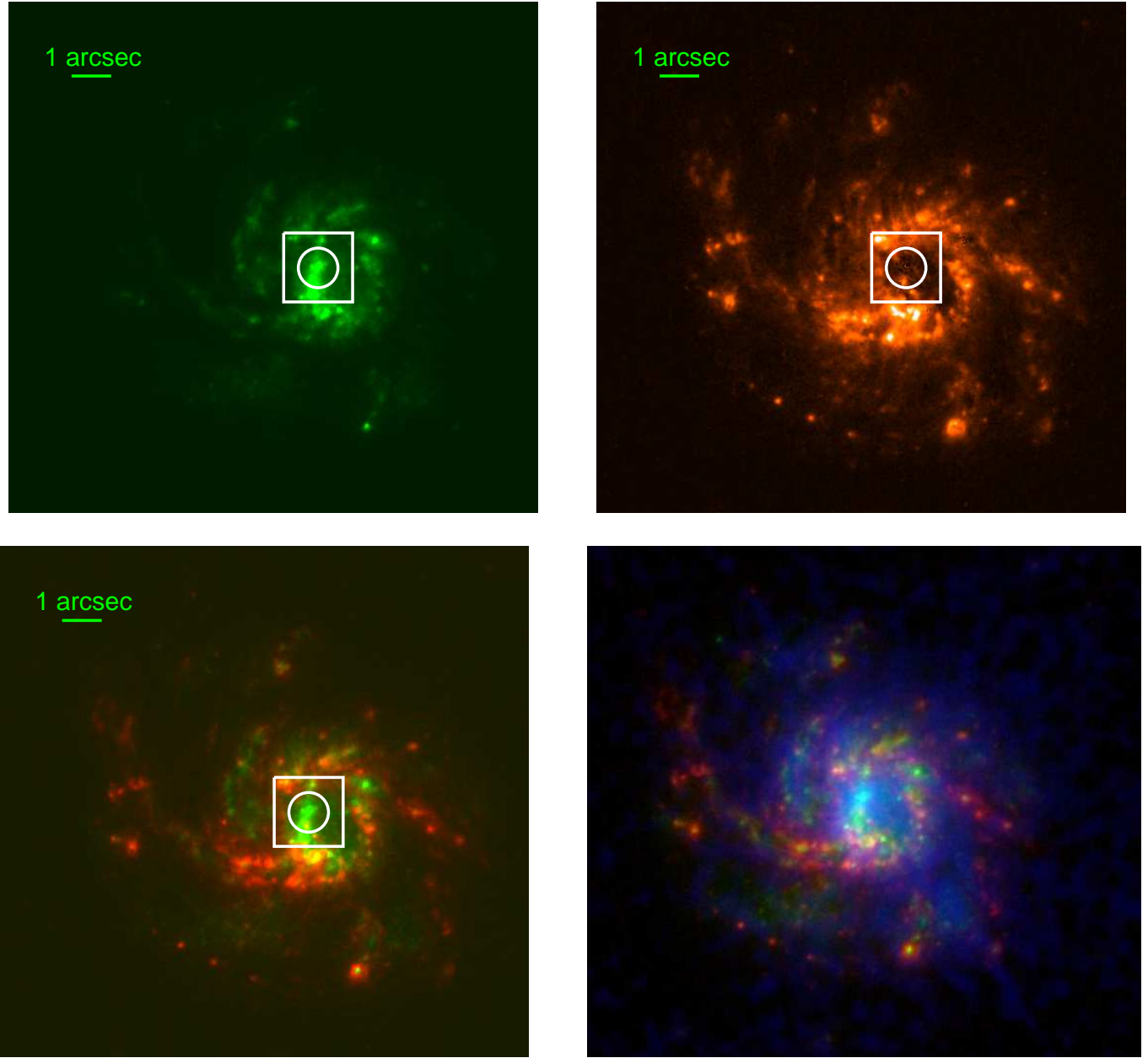


Fig. 4. HST/ACS images of IRAS 0833 in the ultraviolet (filter F140LP, green, *top left*), continuum-subtracted $H\alpha$ (red, *top right*), the composite of both (*bottom left*), and the composite including $Ly\alpha$ emission in blue (*bottom right*, adapted from Östlin et al. (2009)). The aperture of HST/GHRS is marked with a square. The circular region R_1 (radius $\sim 0.5''$ (~ 200 pc)), as discussed in the text, is also marked. Intensity scale is linear, except for the last image, which is logarithmic. North is up and east is left.

high-resolution UV spectra generated with the SB99 models. As shown in Fig. 2 and as already discussed above, whereas the HST/GHRS spectrum only covers the central stellar cluster of IRAS 0833, the low-resolution IUE spectrum contains most of the integrated UV emission of IRAS 0833 (STB). Both the Milky Way and the LMC/SMC libraries were used in the SB99 models, assuming a Salpeter IMF ($\phi(m) \sim m^{-2.35}$) with mass limits of $2 - 120 M_{\odot}$ and $Z = 0.008$ for the evolutionary tracks and the high-resolution spectra. The metallicity value considered was the closest available to the observed one (López-Sánchez et al. 2006). We started by fitting the GHRS spectrum of the SSC, given that its higher spectral resolution allows a more detailed analysis than the IUE one. We checked that no acceptable fitting was possible for the C IV lines with the Milky Way library.

The model that reproduces more accurately the spectral profile of the lines is an instantaneous burst (IB) model of age ~ 5.5 Myr obtained with the LMC/SMC library, in agreement with the age range $4 - 6$ Myr found by López-Sánchez et al. (2006). Furthermore, these authors detected the presence of WR stars within an aperture similar to the HST/GHRS one, with a ratio $WR/(WR + O) \sim 0.03$. According to evolutionary synthesis models (Schaerer & Vacca 1998; Cerviño & Mas-Hesse 1994) the presence of WR stars at the metallicity of IRAS 0833 is only possible if the prompt star forming event is younger than around 6 Myr. The measured $WR/(WR + O)$ ratio is consistent with the predictions for a starburst at $5 - 5.5$ Myr (Schaerer & Vacca 1998). Even more, the $WR/(WR + O)$ value is incompatible with an extended starburst (EB) which had been producing stars for

more than 10 Myr, since then it would show much lower values ($WR/(WR + O) < 0.009$ (Cerviño & Mas-Hesse 1994)). Both the observational HST/GHRS and the SB99 normalized spectra around the Si IV $\lambda\lambda 1394, 1403$ Å and C IV $\lambda\lambda 1548, 1551$ Å lines are shown in Fig. 5 (left panel).

Finally, we checked that the normalized IUE spectrum of STB is consistent with the age obtained from the GHRS data of the SSC region, as far as the lower IUE spectral resolution allows. Though we can not exclude some age spread of the star-forming knots along the spiral arms, we conclude that the global star formation episode in IRAS 0833 is compatible with a short-lived burst which started ~ 5.5 Myr ago over the whole galaxy.

3.3. Extinction

We derived the average reddening of the integrated UV emission of IRAS 0833 (STB) by fitting the IUE spectrum with the SB99 model computed above. The fit was performed by applying a certain intrinsic $E(B-V)$ value to the predicted continuum. The spectrum was then redshifted ($z = 0.0191$) and finally reddened again assuming $E(B-V) = 0.094$ and Cardelli extinction law (Cardelli et al. 1989) to account for the Galactic extinction. The procedure was repeated for different intrinsic $E(B-V)$ values until the observed UV slope and shape were satisfactorily reproduced. As can be seen in Fig. 6 the IUE spectrum of IRAS 0833 shows a prominent 2175 Å feature, typically associated in the past to graphite in the dust grains, but whose origin might be rather in hydrogenated amorphous carbon materials (Gadallah et al. 2011). The SMC law (Prévot et al. 1984) was not considered to model the intrinsic extinction since it does not reproduce the 2175 Å bump, unlike the LMC (Fitzpatrick 1985) and Galactic laws (Cardelli et al. 1989). We assumed $R_V = 3.1$ for these laws. Once the reddening correction was applied, we computed the mass of the integrated source by dividing the observed UV flux at ~ 1529 Å (~ 1500 Å rest frame) by the reddened, redshifted value predicted by the SB99 model. The best fit yielded $E(B-V) = 0.15$ assuming an LMC-like law and $M \sim 1.4 \times 10^8 M_\odot$ for the initial mass of stars (in the 2–120 M_\odot range) having formed all over IRAS 0833 around 5–6 Myr ago. This value of the extinction is in agreement with González Delgado et al. (1998) who obtained $E(B-V) = 0.17$ with an LMC law when fitting the integrated continuum emission observed with HUT (Hopkins Ultraviolet Telescope). When assuming the Cardelli Galactic law for the internal extinction, either the 2175 Å feature or the UV slope at $\lambda < 1800$ Å was reproduced, but not both simultaneously. As shown in Fig. 6 (left panel), the best fit is obtained using the LMC law for the internal extinction, although the 2175 Å is not completely reproduced. If Cardelli law is assumed, $E(B-V)=0.20$ would be required, but the fits neither improve, nor reproduce correctly the slope of the UV continuum. Leitherer et al. (2013) measured $E(B-V)=0.25$ when fitting the spectrum of IRAS 0833 obtained with HST/COS (circular aperture with $radius = 1.25''$), which only includes the spectral range 1100 – 1450 Å. This fit is significantly worse than the one achieved with the LMC law and $E(B-V)=0.15$ when the whole UV range is considered. We want to stress that, contrary to the optical range, different $E(B-V)$ values are required to get the same extinction factor in the UV for different laws.

The reddening affecting the UV continuum of the central stellar cluster in IRAS 0833 (SSC) was also computed by fitting the HST/GHRS spectrum with the predicted SB99 SED, obtaining a very low extinction with $E(B-V) = 0.01$. We assumed an LMC-like extinction law, as derived from the IUE spectrum. The

observed UV continuum, together with the best fitting, reddened SB99 model, have been plotted in Fig. 5 (right panel). Assuming this extinction, the UV continuum emitted by the SSC is compatible with a burst at 5.5 Myr with an initial mass of $M \sim 7.0 \times 10^6 M_\odot$, within the assumed mass limits of 2 – 120 M_\odot .

The values for the best fits are given in Tables 5 and 6, including the reddening and mass values for both the STB and SSC regions. Also, the ratios of the UV and H α emissions and the masses of SSC over STB, i.e. the central region over the integrated IRAS 0833, are included. The compact nature and the mass value of the central stellar cluster in IRAS 0833 indicates that it must be considered a Super Stellar Cluster (Adamo et al. 2010), hence its name SSC. As shown in Table 6, whereas the SSC contributes up to 20% to the total observed UV flux, its intrinsic UV emission accounts for only 5% of the integrated unreddened value. This means that around 5% of the mass within STB is associated to the SSC. Finally, in Fig. 7 we show the HST/GHRS spectrum, together with the IUE one. Also, the predicted SB99 model ($age = 5.5$ Myr, $Z = 0.008$) is included, which has been reddened only by the Galactic extinction ($E(B-V) = 0.094$). As can be seen, the stellar continuum from the SSC is hardly affected by dust extinction, showing a slope similar to the unreddened SB99 model, unlike the STB continuum, which actually shows a positive UV slope below 1500 Å.

3.3.1. Differential extinction

Using NOT/ALFOSC, López-Sánchez et al. (2006) obtained an H α image of IRAS 0833, as well as a spectral image using ALFOSC in spectrographic mode with a $6.4' \times 1''$ slit placed on the center of the source and with a position angle $PA = 138^\circ$. Since the spectral range extended from 3200 to 6800 Å, López-Sánchez et al. (2006) could calculate the Balmer decrement and hence the nebular dust extinction. They obtained an integrated value of $C(H\beta) = 0.22$ for the nebular extinction (see Mazzarella & Boroson (1993) for the definition of $C(H\beta)$), which corresponds to $H\alpha/H\beta = 3.4$ including also the Galactic contribution. This translates into an internal nebular extinction of $E(B-V)=0.06$. On the other hand, these authors found that the nebular extinction is largest within the central region $\sim 1'' \times 1''$ (~ 400 pc \times 400 pc), with $C(H\beta) = 0.30$ (corresponding to $E(B-V) \sim 0.11$ after correction from Galactic extinction).

The effect is reversed when we look at the extinction affecting the stellar continuum. As shown in Fig. 7, while the integrated stellar UV continuum from STB is severely affected by dust, with a global $E(B-V) \sim 0.15$ (corrected from Galactic extinction), the stellar continuum from SSC shows a very low, almost negligible extinction ($E(B-V) \sim 0.01$).

Furthermore, Fig. 4 shows that the H α emission is concentrated in circumnuclear blobs around the central cluster and in the spiral arms, but is very weak just on top of it. The origin of these apparent discrepancies is related to the cavity apparently devoid of gas and dust which surrounds the central SSC. The mechanical energy released by the SSC in the form of stellar winds and supernova explosions has efficiently swept out the gas and dust, leaving a rather clean region just around the central SSC. This explains the low reddening affecting the UV continuum and the lack of H α emission in the close vicinity of the SSC. These stellar winds have apparently concentrated the dust and gas at larger distances (but still close to the SSC), so that the H α emission integrated over this central region appears severely obscured. Outside this central region, the distribution of dust is smoother. In Fig. 8 the spatial profile of H α /H β as derived from

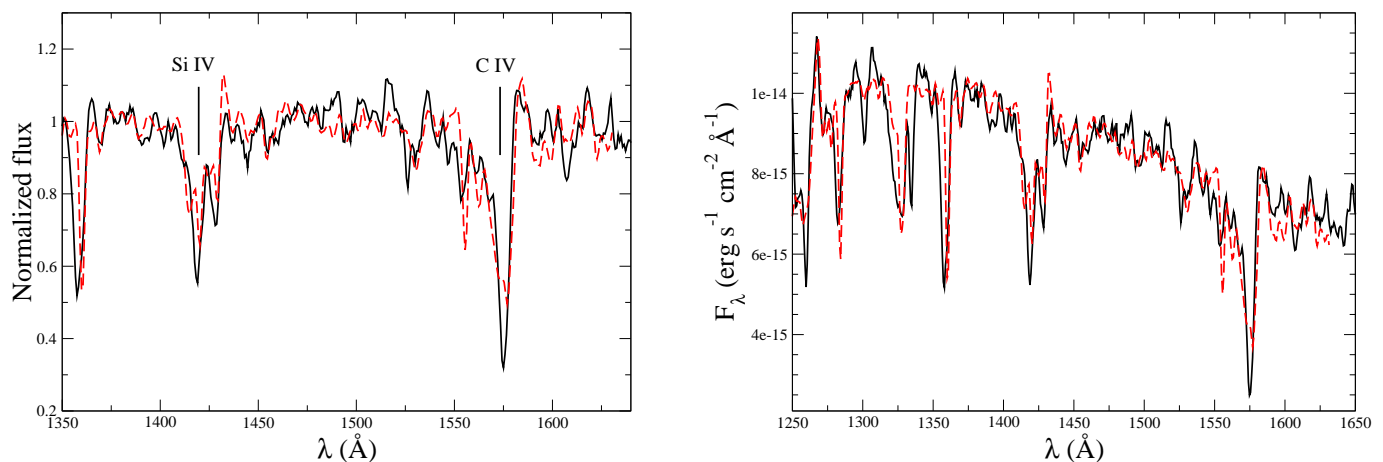


Fig. 5. HST/GHRS spectrum of SSC in IRAS 0833 (solid line) fitted with an SB99 IB model for an age of ~ 5.5 Myr (dashed line). Left: Normalized spectrum with absorption lines Si IV $\lambda\lambda 1394, 1403$ Å and C IV $\lambda\lambda 1548, 1551$ Å labelled. Right: regular spectrum reddened to account for Galactic (Cardelli extinction law, $E(B-V)=0.094$) and intrinsic (LMC law, $E(B-V)=0.01$) extinctions.

the WHT/ISIS observations is shown to be quite uniform over large areas, with just a weak gradient from north to south. This scenario exemplifies the spatial decoupling between the extinction affecting the stellar continuum and that affecting the nebular lines, which is very frequent in starburst galaxies and can yield misleading conclusions when analyzed globally (see further discussion below in Sect.4.1).

3.4. Far infrared emission

Once the starburst in IRAS 0833 had been characterized and its main properties constrained, we checked whether the FIR and $H\alpha$ luminosities from STB could also be reproduced. For this task we used the evolutionary synthesis models by CMHK02 models, which allow to compute the expected FIR flux for a given burst and a specific extinction. López-Sánchez et al. (2006) reported an integrated $H\alpha$ luminosity $L(H\alpha) = 1.2 \times 10^{42}$ erg s $^{-1}$ already corrected for N [II] contamination and internal and Galactic extinctions. Assuming the starburst model described above, the expected intrinsic $H\alpha$ emission predicted by CMHK02 models for STB in IRAS 0833 is $L(H\alpha) = 1.8 \times 10^{42}$ erg s $^{-1}$, which is around 50% higher than the observed value.

This disagreement might be due to the value we have assumed for the fraction f of ionizing photons emitted by the massive stars of STB which are considered to contribute to ionization. Hitherto we have assumed when using the predictions by the CMHK02 models that 30% ($1 - f = 0.3$) of ionizing photons are absorbed by dust before they ionize any hydrogen atom. Mathis (1971) and Petrosian et al. (1972) obtained analytical expressions of f as a function of the optical depth τ . Assuming the latter expression Degioia-Eastwood (1992) obtained values $1 - f \sim 0.3$ for regions in LMC, similar to those found by Mezger (1978) in the Galaxy. According to these results CMHK02 models assume as an average value $(1 - f) = 0.3$ when calculating the intensities of the nebular lines from the predicted number of ionizing photons produced by the massive stars of the burst. However, values measured for τ have uncertainties and might have a spread, which translates into a spread in the parameter $1 - f$. Actually, when assuming $1 - f = 0.5$, CMHK02 models predict a value for $H\alpha$ luminosity in IRAS 0833 in agreement with the value reported by López-Sánchez et al. (2006). This value of $1 - f$ is realistic, indeed similar to the fraction measured in sev-

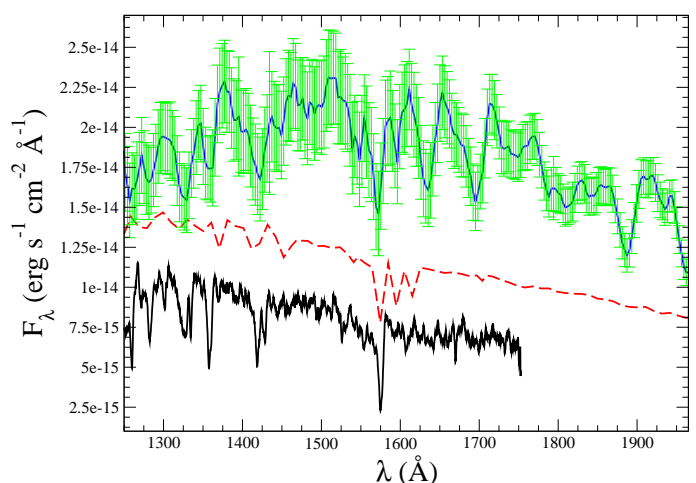


Fig. 7. Observed HST/GHRS (black, solid line, SSC) and IUE (blue, solid, STB; errors in green) spectra, together with the SB99 model for an age of 5.5 Myr (red, dashed). Vertical scale corresponds to the GHRS spectrum. The other spectra have been arbitrarily scaled for an easier comparison. SB99 model has been corrected only for Galactic extinction.

eral Galactic H II regions (Mezger 1978), and consistent with the rather high value of extinction measured in the STB spectrum.

Infrared emission $FIR(40 - 120 \mu\text{m})$ was calculated using the relation by Helou et al. (1985) based on the IRAS fluxes $F_{60 \mu\text{m}} = 5.81$ Jy and $F_{100 \mu\text{m}} = 6.48$ Jy. Following Calzetti et al. (2000), the value of $FIR(40 - 120 \mu\text{m})$ was converted to the estimated total far infrared emission with the relation $FIR(1 - 1000 \mu\text{m})/FIR(40 - 120 \mu\text{m}) \sim 1.75$. The resulting value is $L_{FIR} = 3.6 \times 10^{44}$ erg s $^{-1}$. Assuming $E(B-V) = 0.15$ with the LMC extinction law and $1 - f = 0.5$, CMHK02 models predict $L_{FIR} = 4.2 \times 10^{44}$ erg s $^{-1}$ for STB. Though the predicted L_{FIR} value is higher by 16% than the observed one, both values are consistent considering the inherent uncertainties of the method, and the systematic $\pm 10\%$ uncertainty in the predicted luminosities discussed above. All the predicted and observed values are shown in Table 5.

The rather good agreement between the predicted and observed values of $L(H\alpha)$ and L_{FIR} , with a general trend to some overestimation by the models, indicates that the UV continuum

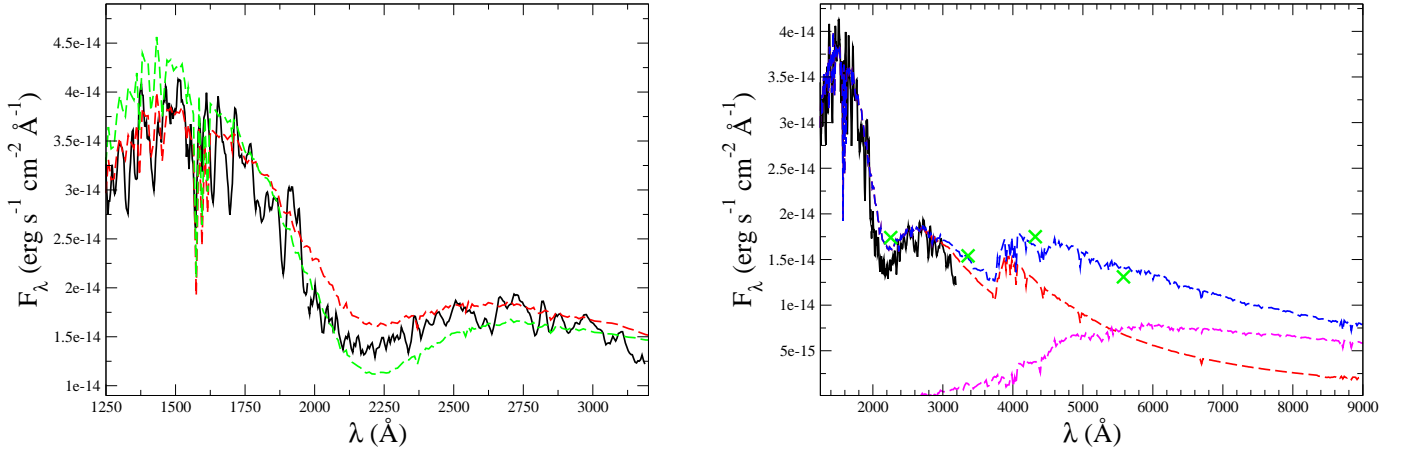


Fig. 6. **Left:** IUE spectrum of STB in IRAS 0833 (black, solid line) fitted with an SB99 spectrum for an age of 5.5 Myr (dashed lines). The model has been reddened to account for the Galactic extinction, as well as for the intrinsic one assuming both an LMC law and $E(B-V)=0.15$ (red), and the Cardelli extinction law with $E(B-V)=0.20$ (green). **Right:** IUE spectrum is shown as in the left panel (black, solid line). A composite model (blue, dashed line) was obtained summing the starburst model (red) and an SB99 spectrum of a 1-Gyr-old population reddened similarly as the young burst model (magenta, dashed line). Near-UV and optical photometric fluxes from Östlin et al. (2009) are marked with green crosses.

Table 5. Predicted values of the age, mass, stellar and nebular extinctions, fraction of ionizing photons absorbed by dust, emission fluxes and luminosities and $EW(H\beta)$ of the starburst (STB) in IRAS 0833, assuming the UV fluxes from HST/ACS and IUE and the average value of both. The Galactic extinction effect has been removed from the $E(B-V)$ values, which thus strictly correspond to the intrinsic extinction within the source. Contribution to the optical continuum by old stars was considered when estimating $EW(H\beta)$ (see Sect. 3.5 for details). Observed values are also shown.

	Age (Myr)	M (M_{\odot})	$E(B-V)_*$	$E(B-V)_{\text{neb}}$	$1-f$	F_{1529} ($\text{erg s}^{-1} \text{cm}^{-2} \text{\AA}^{-1}$)	L_{1500}^a ($\text{erg s}^{-1} \text{\AA}^{-1}$)	$L(H\alpha)^a$ (erg s^{-1})	L_{FIR} (erg s^{-1})	$EW(H\beta)$ (\AA)
Model(ACS)	5.5	1.5×10^8	0.15	0.06	0.5	4.8×10^{-14}	3.2×10^{41}	1.3×10^{42}	4.5×10^{44}	14
Model(IUE)	5.5	1.3×10^8	0.15	0.06	0.5	4.1×10^{-14}	2.7×10^{41}	1.2×10^{42}	3.8×10^{44}	14
Model(average)	5.5	1.4×10^8	0.15	0.06	0.5	4.5×10^{-14}	3.0×10^{41}	1.2×10^{42}	4.2×10^{44}	14
Observed	-	-	0.17 ^b	0.06 ^c	-	4.5×10^{-14}	3.0×10^{41}	1.2×10^{42} ^c	3.6×10^{44}	19 ^c

^a Luminosity value corrected for Galactic and intrinsic extinctions.

^b Value from González Delgado et al. (1998).

^c Value from López-Sánchez et al. (2006).

Table 6. Observed values of the UV and $H\alpha$ emissions and the stellar and nebular extinctions of the integrated source IRAS 0833 (STB) and its central stellar cluster (SSC), together with the predicted stellar mass for each of them. The Galactic extinction effect has been removed from the $E(B-V)$ values, which thus strictly correspond to the intrinsic extinction within the source. The mass of the central region SSC was obtained from the UV intrinsic luminosity. Ratios between values for each region are also shown.

Name	Region	$E(B-V)_*$	$E(B-V)_{\text{neb}}$	F_{1529} ($\text{erg s}^{-1} \text{cm}^{-2} \text{\AA}^{-1}$)	L_{1500}^a ($\text{erg s}^{-1} \text{\AA}^{-1}$)	$L(H\alpha)^a$ (erg s^{-1})	M (M_{\odot})
STB	Integrated source	0.15	0.06	4.5×10^{-14}	3.0×10^{41}	1.2×10^{42}	1.4×10^8
SSC	Central stellar cluster	0.01	0.11	8.5×10^{-15}	1.5×10^{40}	1.3×10^{41}	7.0×10^6
Ratio (SSC/STB)	-	-	-	20%	5%	10%	5%

^a Luminosity value corrected for Galactic and intrinsic extinctions.

(used for normalization) is contributed by the complete population of young stars in the central region of IRAS 0833. Therefore, there are no evidences of additional stellar knots potentially hidden within dense dust clouds, which would be invisible in the UV, but would contribute to $L(H\alpha)$ and L_{FIR} , as found in other similar galaxies like Haro 2 (Otí-Flóranes et al. 2012).

3.5. Underlying stellar population

Leitherer et al. (2013) considered that the HST/COS aperture was large enough ($\text{radius} = 1.25''$) to contain short-lived massive bursts at different ages, mimicking a quasi-continuous star formation rate, and adopted a characteristic age of 20 Myr. The detection by Pellerin & Robert (1999) of the

Ca II $\lambda\lambda 8498, 8542, 8662$ Å and Mg₂ $\lambda 5177$ Å absorption lines in an IR-optical spectrum of the source, which are signatures of red (super)giants (RSGs) and late-type stars, respectively, supported in principle this assumption, since the presence of both O stars and RSGs requires starbursts extended over at least ~ 10 Myr. Nevertheless, Pellerin & Robert (1999) attributed the strength of the Ca II triplet and Mg₂ absorption lines to an old stellar population of ≥ 1 Gyr, rather than to young RSGs. As discussed by López-Sánchez et al. (2006) it is known that IRAS 0833 has experienced previous star-formation episodes, with at least two older stellar populations with ages 100 – 200 Myr and 1 – 2 Gyr, respectively. Mas-Hesse et al. (2003) showed in their Fig. 11 that the optical continuum peaks $\sim 1.2''$ (~ 470 pc) north from a high-intensity emitting ionized gas within the STIS slit. This region (which they labelled “N”) presents a strong Balmer discontinuity and a lack of ionizing power, and is consequently dominated by older stars. We argue that, as we discuss below, the stars in this region and other similar ones are dominating the features detected by Pellerin & Robert (1999), but do not have any relation with the young starburst in the core of IRAS 0833.

Moreover, when we tried to reproduce the different observables assuming synthesis models for extended bursts with the parameters considered by Leitherer et al. (2013), the Si IV and C IV spectral profiles could not be simultaneously fitted, and the stellar mass value which would account for the UV emission from STB overestimated the predicted $L(H\alpha)$ and L_{FIR} by factors 7 and 3, respectively. As discussed above, the measured $WR/(WR + O)$ ratio is neither consistent with an extended starburst. Therefore, our results reject the hypothesis of a star formation episode extended over several tens of Myr in IRAS 0833. We conclude that the Balmer lines emission, the UV continuum and the far infrared luminosity are dominated by a starburst which converted $\sim 1.4 \times 10^8 M_{\odot}$ of gas into stars ~ 5.5 Myr ago. As already explained, our data do not allow us to constrain the age of the young, massive stars contributing to the UV continuum outside the central bar SSC, but the good fit with the lower resolution global IUE spectrum indicates that the spread in ages has to be very small. In addition, an underlying, older stellar population which dominates the optical to infrared continuum must have been formed in previous star formation episodes distributed over the last 1 Gyr.

In order to check this assumption, we plotted in Fig. 6 (right panel) the UV-optical SED of IRAS 0833. It includes the IUE spectrum already fitted in the left panel and discussed in the text, as well as the photometric fluxes obtained by Östlin et al. (2009) from HST/ACS observations. We noticed that the same model described in Table 5 and which can reproduce the UV slope and the UV, $H\alpha$ and FIR emissions from STB, was unable to account for the SED at $\lambda \gtrsim 4000$ Å. Since there are evidences of the presence of an older stellar population, as discussed above, we included a 1-Gyr-old SB99 model with same metallicity and mass limits as for the young starburst. This spectrum was reddened by the same amount than the IUE continuum to account for internal ($E(B-V) = 0.15$, LMC law) and Galactic ($E(B-V) = 0.094$, Cardelli law) extinctions. As shown in Fig. 6, whereas the young starburst population dominates the UV emission, the composite of the old and young populations reproduces properly the optical fluxes reported by Östlin et al. (2009) when $M_{old} = 6 \times 10^{10} M_{\odot}$.

We have considered only a test case assuming a model for an age of 1 Gyr. The results do not vary significantly for other configurations, so that we can conclude that a stellar population some hundreds of Myrs old contributes significantly to the optical-IR continuum observed in IRAS 0833. Indeed, Fig. 6

shows that the continuum at $\lambda \sim 8500$ Å is dominated by the older stars, which therefore must account for the Ca II triplet absorption lines, as suggested by Pellerin & Robert (1999). Finally, when considering the contribution by the old stellar population, CMHK02 models predict $EW(H\beta) \sim 14$ Å for the integrated starburst in IRAS 0833. Bearing in mind the uncertainties in the actual contribution of the underlying stellar population to the stellar continuum, as well as the effect of extinction in its optical emission, this $EW(H\beta)$ estimate is in agreement with the value $EW(H\beta) = 19$ Å reported by López-Sánchez et al. (2006). The $EW(H\beta)$ calculated from the models, as well as the observed value, are included in Table 5.

In brief, the UV, $H\alpha$ and FIR emissions in IRAS 0833 are dominated by the young stars produced in a starburst which occurred ~ 5.5 Myr ago, which took place all along the central region of the galaxy, as well as in the surrounding spiral arms. On the other hand, the optical-IR continuum, as well as other features such as the Ca II triplet, are mostly contributed by old stars formed some hundred millions years before the current starburst took place.

3.6. Ly α emission

A high-resolution spectrum around Ly α of the central region of IRAS 0833 is shown in Fig. 10. This 1-d spectrum was extracted by Mas-Hesse et al. (2003) from the HST/STIS G140M spectral image, which is shown in Fig. 8 (top panel). The Ly α emission is very prominent, extending well beyond the stellar continuum to the north direction, whereas the emission toward the south is much weaker. Unlike what Oti-Floranes et al. (2012) found on the major axis of Haro 2, regions of total Ly α absorption are not observed along the slit. The Ly α spatial profile in Fig. 8 (middle panel) shows two compact components at both sides of the central cluster: north peak (*position* $\sim -0.7'' \sim -300$ pc, *width* $\sim 1'' \sim 400$ pc, $F \sim 4 \times 10^{-16}$ erg s⁻¹ cm⁻²), and south peak (*position* $\sim 1'' \sim 400$ pc, *width* $\sim 1.5'' \sim 600$ pc, $F \sim 6 \times 10^{-16}$ erg s⁻¹ cm⁻²). In the region between them there is an abrupt decline, which is co-spatial to the stellar cluster. Also, a somewhat diffuse emission is observed extending to the north (*position* $< -1'' \sim 400$ pc) over $\sim 6''$ (~ 2.3 kpc), and with a lower flux ($F < 2 \times 10^{-16}$ erg s⁻¹ cm⁻²). On the other hand, the emission extending south from the southern peak is much weaker. The total spatial extension of the Ly α emission is $\sim 16''$ (~ 6 kpc), whereas the stellar continuum, dominated by the central stellar cluster, extends over $\sim 5''$ (~ 1.9 kpc). The observed, integrated flux of Ly α along the STIS slit is $F(Ly\alpha) \sim 6.4 \times 10^{-14}$ erg s⁻¹ cm⁻² (not corrected for any kind of absorption or extinction), with the diffuse emission contributing up to $\sim 25\%$ of the total one.

Figures 8 and 10 show also a deep, broad Ly α absorption bluewards of the emission. Mas-Hesse et al. (2003) concluded that this P Cyg profile was consistent with scattering by a neutral medium outflowing at ~ 300 km s⁻¹. A weak secondary Ly α emission component is observed onto the deep absorption trough. This emission is also blueshifted by ~ 300 km s⁻¹. Moreover, this secondary emission extends along $\sim 6.0''$ (~ 2.3 kpc), with a total observed flux of $F(Ly\alpha) \sim 5.5 \times 10^{-15}$ erg s⁻¹ cm⁻². Figure 9 shows the spatial profile of the main and secondary Ly α components, together with the profile of the UV continuum. As observed, although ~ 10 times weaker, the secondary Ly α emission roughly follows the spatial profile of the primary component, except for the peak $\sim 1''$ north of the central cluster, which

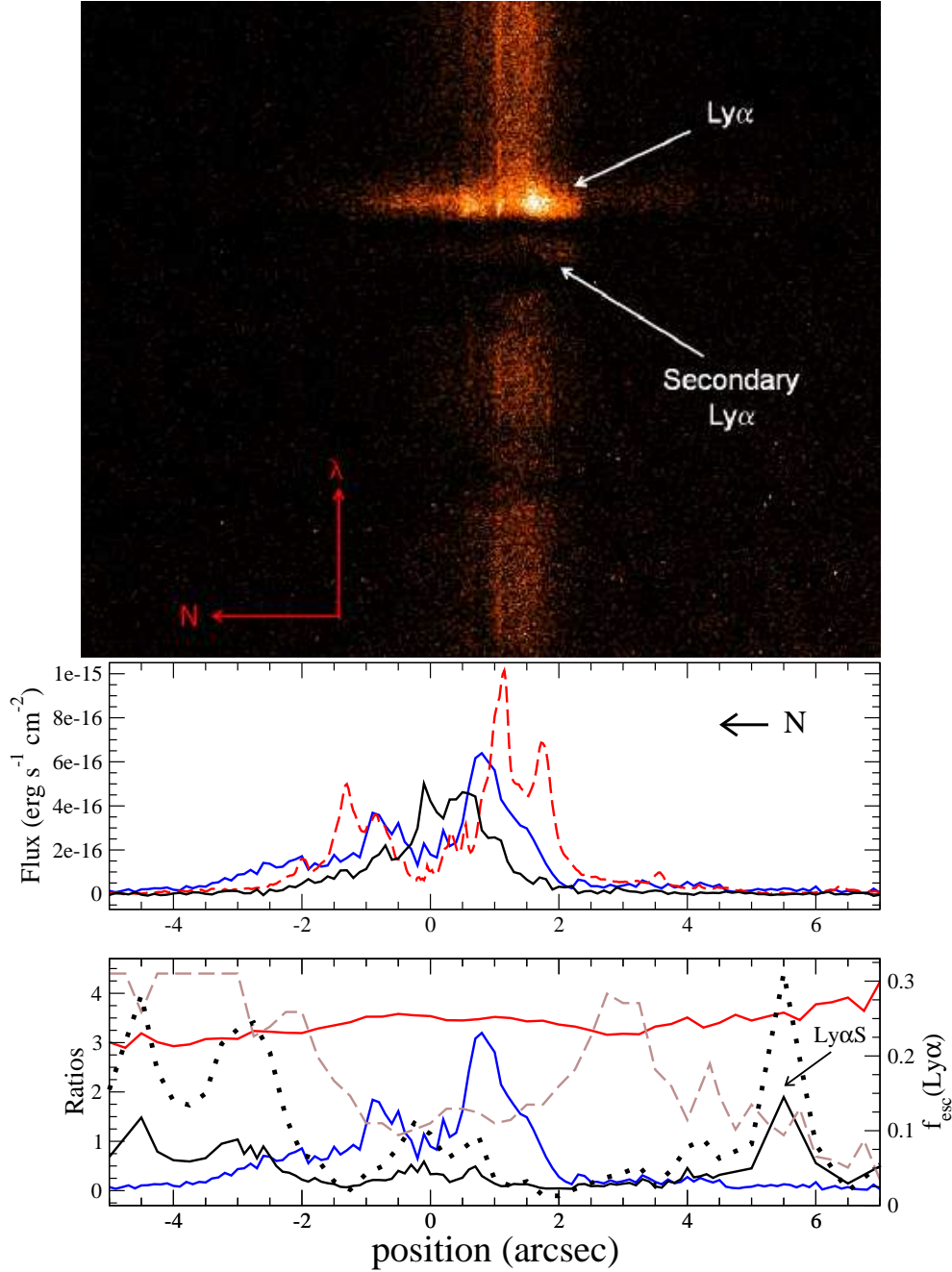


Fig. 8. **Top:** HST/STIS G140M spectral image of IRAS 0833. Spatial extension is $\sim 19''$ (~ 7.5 kpc). **Middle:** emission profile of the main component of Ly α (blue) and UV continuum (1224.5 \AA rest frame, black) from STIS data, and H α (red-dashed) from ACS data. **Bottom:** spatial profiles of Ly α (blue) and observed Ly α /H α (solid black) and H α /H β (from WHT/ISIS data, in red), and the expected Ly α /H α ratio (brown-dashed), assuming Case B recombination and internal reddening as derived from the H α /H β ratio, as well as the Galactic extinction. The Ly α escape fraction $f_{\text{esc}}^{\text{Ly}\alpha}$, as defined in the text, has been plotted in black-dotted line. In the middle and bottom panels the negative x -axis corresponds to north, as indicated by N . To ease the comparison, the red dashed line in the middle panel shows the H α profile scaled by a factor 0.2. The vertical scale corresponds to the Ly α and non-scaled H α fluxes. Whereas the vertical scale of the left axis in the bottom panel corresponds to the Ly α /H α and H α /H β ratios, the scale of the right axis corresponds to $f_{\text{esc}}^{\text{Ly}\alpha}$. Position of the region Ly α S is marked.

is not observed in the former. Both emissions are spatially decoupled from the stellar continuum.

Mas-Hesse et al. (2003) found the same velocity structure in the P Cyg profile of the Ly α emission detected in IRAS 0833 all along the STIS slit, i.e. over at least $10''$ (~ 4 kpc). They found that the profiles fall to zero at the same velocities within a narrow range ($\pm 50 \text{ km s}^{-1}$), regardless of the distance to the central region. Therefore, these observations indicate that most of the

neutral gas responsible for the absorption feature must be approaching us at the same velocity $\sim 300 \text{ km s}^{-1}$ all along the slit.

3.7. X-rays

As explained above, the analysis of the X-ray data of IRAS 0833 was performed using *XSPEC*. The complexity of each model was

Table 7. X-ray spectral fitting of IRAS 0833, with the number of degrees of freedom (ν) and the reduced χ^2 value (χ^2/ν).

Model	kT (keV) Norm ^a	kT (keV) / Γ Norm ^a	Metallicity Z_{\odot}	ν	χ^2/ν
1: wabs*zwabs*(zmekal+zmekal)	$0.60^{+0.06}_{-0.11}$ $6.0^{+1.1}_{-1.1} \times 10^{-5}$	$4.2^{+1.7}_{-1.0}$ $1.44^{+0.18}_{-0.18} \times 10^{-4}$	0.4	37	1.056
2: wabs*zwabs*(zmekal+zpowerlw)	$0.62^{+0.08}_{-0.11}$ $4.6^{+1.4}_{-1.5} \times 10^{-5}$	$2.0^{+0.2}_{-0.2}$ $4.9^{+1.0}_{-0.9} \times 10^{-5}$	0.4	37	0.993

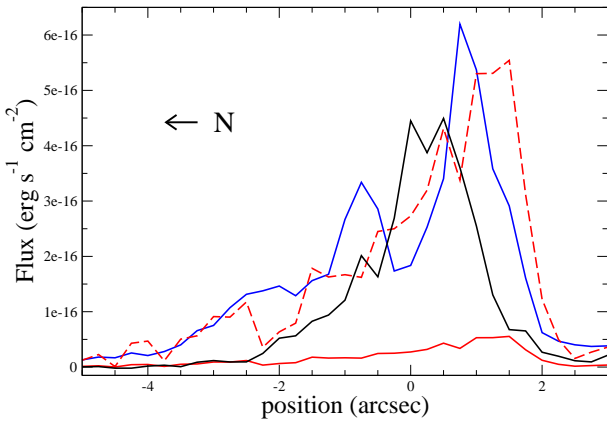
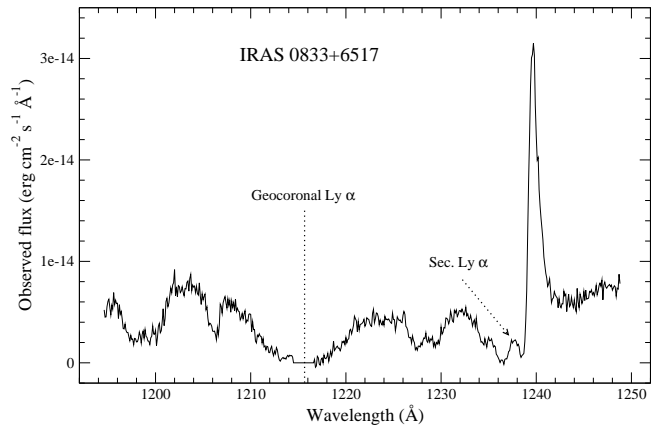
^a Units of normalization as in XSPEC. Hot plasma: $10^{-14} / \{4\pi [D_A(1+z)]^2\} \int n_e n_H dV$. Power-law: photons $s^{-1} cm^{-2} keV^{-1}$ (1 keV).

Table 8. X-ray fluxes and luminosities of IRAS 0833, together with the fractional contribution to the soft X-ray range by the harder spectral components.

Model	$F_{0.4-2.4 keV}$ ^a (erg $s^{-1} cm^{-2}$)	$F_{2.0-10.0 keV}$ ^a (erg $s^{-1} cm^{-2}$)	$L_{0.4-2.4 keV}$ ^b (erg s^{-1})	$L_{2.0-10.0 keV}$ ^b (erg s^{-1})	$L_{0.4-2.4 keV}^{HXcomp} / L_{0.4-2.4 keV}^{tot}$ ^b
1: wabs*zwabs*(zmekal+zmekal)	$1.49^{+0.08}_{-0.09} \times 10^{-13}$	$1.13^{+0.18}_{-0.3} \times 10^{-13}$	$1.36^{+0.08}_{-0.08} \times 10^{41}$	$8.7^{+1.4}_{-2} \times 10^{40}$	$0.60^{+0.07}_{-0.07}$
2: wabs*zwabs*(zmekal+zpowerlw)	$1.58^{+0.11}_{-0.11} \times 10^{-13}$	$1.2^{+0.2}_{-0.2} \times 10^{-13}$	$1.47^{+0.10}_{-0.10} \times 10^{41}$	$9.3^{+1.7}_{-1.5} \times 10^{40}$	$0.71^{+0.11}_{-0.09}$

^a Values of fluxes have not been corrected for neutral absorption.

^b Values of luminosities have been corrected for neutral absorption.

**Fig. 9.** Emission profiles of the UV continuum (1224.5 Å rest frame, black), primary Ly α (blue) and secondary Ly α (red) emissions from HST/STIS data. The vertical scale corresponds to the Ly α flux. The secondary emission has been scaled by a factor 10 (red dashed line) to ease the comparison. Spatial resolution of all the profiles was degraded to 0.25 arcsec pixel⁻¹.**Fig. 10.** Extracted 1-d spectrum of the central region of IRAS 0833 (corresponding to 2''). The position of the geocoronal Ly α line has been marked, in the center of the broad Galactic absorption profile. We have also marked the position of the secondary emission peak discussed in the text. Reproduced from Mas-Hesse et al. (2003).

increased once its statistical significance had been checked with respect to the previous more simple one. Changes in the models were considered valid if the probability significance yielded by the F-test was $> 99\%$. Galactic neutral absorption was fixed to $N(H I)_{Gal} = 4.5 \times 10^{20} cm^{-2}$ (see Table 1). The intrinsic neutral hydrogen column density was measured by Kunth et al. (1998) from the Ly α profile, obtaining $N(H I)_{int} = 7.9 \times 10^{19} cm^{-2}$, although the uncertainties were large and this value only corresponds to the line of sight of the central cluster. We studied models with the parameter $N(H I)_{int}$ free, but no improvement on the fitting was obtained over the models with $N(H I)_{int}$ fixed to the value reported by Kunth et al. (1998), which was there-

fore assumed. This is due to the low intrinsic column density of IRAS 0833, which is roughly one order of magnitude lower than the Galactic one. Metallicity was fixed to $Z = 0.4Z_{\odot}$ as measured by López-Sánchez et al. (2006). As explained in Sect. 2.3, models were checked to yield similar values for the parameters for both MOS1 and MOS2 spectra.

Models with only one emitting component did not yield satisfactory fittings. Finally, two models were found for which the fits obtained were acceptable, and which we labelled as Model 1 and Model 2. The former is a two-temperature hot plasma (HP_{soft} and HP_{hard}), modeled by mekal in XSPEC (Mewe et al. 1985).

On the other hand, Model 2 is a composite of a hot plasma and a power-law emission (PL). All components from both models are affected by the Galactic and the intrinsic absorptions. The values of the parameters obtained for each of the models are listed in Table 7, where errors were calculated for a confidence level of 90%. The temperature of HP_{soft} is similar for Model 1 and Model 2 ($0.60^{+0.06}_{-0.11}$ keV and $0.62^{+0.08}_{-0.11}$ keV, respectively), as well as its flux contribution, which indicates that HP_{soft} accounts for the same emission in both models. Only the modeling of the hard emission varies between them, being another hot plasma (HP_{hard}) with $kT = 4.2^{+1.7}_{-1.0}$ keV in Model 1 and a power-law (PL) with $\Gamma = 2.0^{+0.2}_{-0.2}$ in Model 2. When considering a Raymond-Smith model (raymond model in XSPEC (Raymond & Smith 1977)) instead of mekal, a worse fitting was obtained, and thus raymond was rejected.

In Table 8 the values of the fluxes and luminosities for Models 1 and 2 are shown, together with $L_{\text{HXcomp}}^{0.4-2.4\text{ keV}}/L_{\text{tot}}^{0.4-2.4\text{ keV}}$, the fractional contribution to the total soft X-ray (0.4 – 2.4 keV) luminosity by the component dominating the hard X-ray range, i.e. $L_{\text{HPhard}}^{0.4-2.4\text{ keV}}/L_{\text{tot}}^{0.4-2.4\text{ keV}}$ for Model 1, and $L_{\text{PL}}^{0.4-2.4\text{ keV}}/L_{\text{tot}}^{0.4-2.4\text{ keV}}$ for Model 2. Errors correspond to a confidence level of 90%. MOS1 and MOS2 spectra of the source are shown in Fig. 11, together with the fitting Models 1 and 2. Stevens & Strickland (1998) analyzed a ROSAT/SPPC observation and fitted the resulted spectrum of the source with a model of an absorbed hot plasma. Assuming a Galactic column density of $N(\text{H I})_{\text{Gal}} = 4.08 \times 10^{20} \text{ cm}^{-2}$ they obtained $kT = 0.58^{+0.6}_{-0.08}$ keV, $N(\text{H I})_{\text{int}} = 1.4^{+5}_{-1.1} \times 10^{21} \text{ cm}^{-2}$, $Z = 0.02^{+0.2}_{-0.02} Z_{\odot}$, and a value for the soft X-ray luminosity $L_{0.1-2.5\text{ keV}} = 2.8^{+9}_{-1.7} \times 10^{41} \text{ erg s}^{-1}$. Uncertainties are very high since the statistics of the ROSAT spectrum contained only 9 points. Our XMM-Newton data correct downwards the luminosity measured by Stevens & Strickland (1998).

4. Discussion

We have analyzed UV-optical observational data of the local, face-on spiral galaxy IRAS 0833, which hosts an intense Ly α -emitting starburst. We have concluded that the onset of the present starburst occurred ~ 5.5 Myr ago, leading to the production of a total stellar mass of $1.4 \times 10^8 M_{\odot}$. While the stellar UV continuum of the integrated source (STB) is highly reddened by dust, the emission of the super stellar cluster in its core (SSC) barely shows any dust extinction. This irregular distribution of dust causes SSC to account for 5% of the STB mass, but up to 20% of the integrated observed UV flux. IRAS 0833 shows a prominent Ly α emission, with a complex spectral profile featuring two emission peaks. The brightest one shows a clear P Cyg profile due to resonant scattering by neutral gas outflowing at $\sim 300 \text{ km s}^{-1}$. The ~ 10 times weaker secondary Ly α emission is observed on top of the deep saturated absorption trough caused by the neutral hydrogen in the main component. This secondary Ly α emission appears blueshifted by the same velocity $\sim 300 \text{ km s}^{-1}$ as the outflowing neutral gas. Both compact and diffuse Ly α emissions were detected along the slit. Whereas the former is observed in two regions located between the central massive stellar cluster and the H α -emitting structures, the latter was detected extending $\sim 6''$ ($\sim 2.3 \text{ kpc}$) northward from the northern Ly α compact component, with a much weaker diffuse emission extending to the south. Finally, we have analyzed the X-ray spectrum of STB, which is contributed by thermal emission in the soft X-ray range, and a non-thermal power law, or a hotter thermal component, extending also to the hard X-rays. The low spatial

resolution of the X-ray image does not allow to extract any morphological information.

In this section we will discuss the properties of SSC and its surroundings, the origin of the X-ray luminosity from STB, and the distribution of the Ly α emission over the central area of IRAS 0833.

4.1. Central super stellar cluster

We have seen in Fig. 4 that the central super stellar cluster (SSC) in IRAS 0833 shows a conspicuous UV continuum, but a very low local H α emission. Ly α shows also a local minimum at the position of the central SSC, as shown in Fig. 8. To analyze the lack of H α emission in the very inner regions of the IRAS 0833 core, a smaller circular region with $\text{radius} = 0.5''$ ($\sim 200 \text{ pc}$, hereinafter R_1) was considered, which is marked on Fig. 4. We extracted the H α and UV fluxes of R_1 and corrected them for the nebular and stellar dust extinction, respectively, as discussed in Sect. 3.3. For an instantaneous starburst with the properties given in Table 5, and a mass which would account for the UV emission within R_1 ($M \sim 3.1 \times 10^6 M_{\odot}$), CMHK02 models predict a value of $L(\text{H}\alpha) \sim 1.5$ times larger than indeed observed within the aperture, even when assuming $1-f = 0.5$ as discussed above. In brief, around 30% of the ionizing photons emitted by the SSC and not absorbed by dust, are actually escaping from the region.

On the other hand, Fig. 4 and the spatial profiles of the UV continuum and H α emission in Fig. 8 indicate that the emitting nebular gas is mostly located towards the north and the south of the central SSC. Specifically, we observe in Fig. 8 that, whereas the bulk of the stellar cluster continuum is concentrated within $1''$ (400 pc), H α shows two main components: north peak ($\text{position} \sim -1.5'' \sim -600 \text{ pc}$, $\text{width} \sim 1'' \sim 400 \text{ pc}$, $F \sim 2.5 \times 10^{-15} \text{ erg s}^{-1} \text{ cm}^{-2}$), and south peak ($\text{position} \sim 1'' \sim 400 \text{ pc}$, $\text{width} \sim 1.5'' \sim 600 \text{ pc}$, $F \sim 5 \times 10^{-15} \text{ erg s}^{-1} \text{ cm}^{-2}$). The weak H α emission observed at the position of the SSC ($F \sim 2.5 \times 10^{-16} \text{ erg s}^{-1} \text{ cm}^{-2}$) has to be due to the lack of gas within R_1 . As discussed above, the gas has been swept up by the intense starburst activity (stellar winds, SNe, etc.) during the last 5.5 Myr since the onset of the burst, creating a cavity with a $\text{diameter} \sim 1.5''$ ($\sim 600 \text{ pc}$). Outside this cavity H α is actually prominent and structured, resulting from ionization by the local massive stars and by the ionizing photons which escaped from the central region. As already mentioned, the low extinction derived from the stellar continuum in the core SSC indicates that the abundance of dust within the cavity is also very low. These empty, dust-free cavities are usual around strong starbursts, as discussed by Maíz-Apellániz et al. (1998) for NGC 4214. Figure 12 shows in high detail how in these cases the nebular lines are emitted by the gas swept up by the starburst, together with the dust, yielding a strong differential extinction with respect to the stellar cluster, whose line of sight remains almost free of dust and gas.

4.2. X-rays

The low spatial resolution of the X-ray XMM-Newton/EPIC observations, with IRAS 0833 $\sim 8'$ away from the optical axis, did not allow to study its morphology, but just to derive the integrated average physical properties of the emitting gas, as discussed above. The spectral analysis of IRAS 0833 unveiled the contribution by a hard component, which may be thermal (Model 1 in Table 7) or non-thermal (Model 2) in nature, and which in any case contributes up to $\sim 60 - 70\%$ to $L_{0.4-2.4\text{ keV}}$. The rather evolved state of the starburst in IRAS 0833 indi-

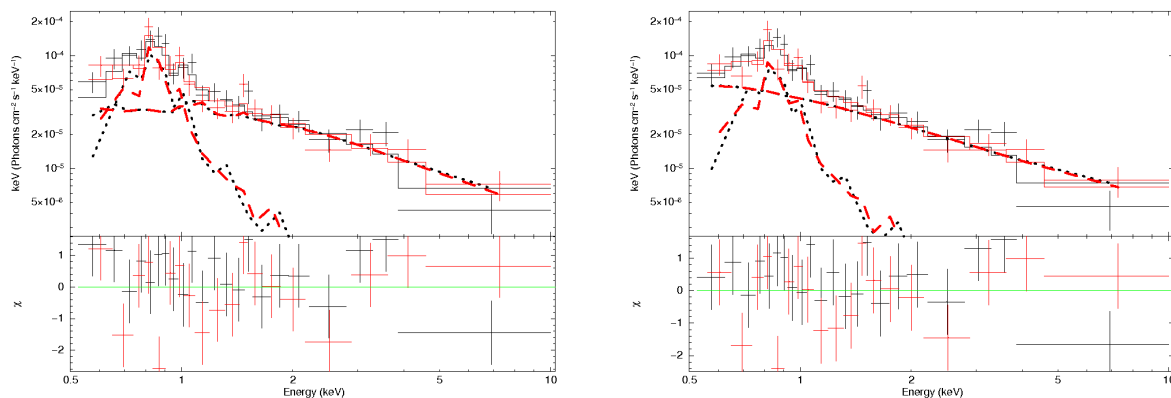


Fig. 11. XMM-Newton/EPIC X-ray spectrum of IRAS 0833 with fitting Model 1 (left) and Model 2 (right). The different components of the models are shown in dashed and dotted lines. MOS1 and MOS2 data are shown, together with the residuals of the fits (lower panels). Model 2 is favoured over Model 1 since it reproduces the hard X-ray emission with a non-thermal component, as predicted by synthesis models

icates that supernova remnants (SNR) should already be present, and that a significant number of binary systems might have already become active as high mass X-ray binaries (HMXBs), i.e. might have started to accrete material onto a compact stellar remnant (black hole or neutron star formed after the SN explosion of its massive, short-lived progenitor). The CMHK02 models predict $N_{SN} \sim 10^{-9} M_{\odot}^{-1} \text{ yr}^{-1}$ (Cerviño & Mas-Hesse 1994), which scales to around 150 SN explosions every 10^3 yr for IRAS 0833, half of which are expected to be part of a binary system. The fraction of them with also a massive secondary, already in its last stages of evolution after 5.5 Myr, should be active as HMXBs. The CMHK02 models predict $\sim 2 \times 10^3$ active HMXBs in IRAS 0833 given the mass and evolutionary status of the starburst (Cerviño et al. 1997). Assuming a typical luminosity of $L_X = 10^{38} \text{ erg s}^{-1}$ for a single HMXB, a contribution of $L_X = 2 \times 10^{41} \text{ erg s}^{-1}$ by HMXBs is expected. This value matches the luminosity contribution of the non-thermal component of Model 2 of Table 7. Furthermore, following the method proposed by Mineo et al. (2012a), based on the calibration of HMXB luminosity function in star-forming galaxies using a composite of L_{FIR} and observed L_{UV} as a proxy, we find that ~ 60 HMXBs with $L_{hardX} > 10^{38} \text{ erg s}^{-1}$ should be currently active in IRAS 0833, providing an integrated hard X-ray luminosity $L_{0.5-8 \text{ keV}} \sim 5 \times 10^{40} \text{ erg s}^{-1}$. While this value is lower than the observed one, $L_{0.5-8 \text{ keV}} \sim 2 \times 10^{41} \text{ erg s}^{-1}$, it is within 1σ of the dispersion in the sample by Mineo et al. (2012a). We conclude therefore that the hard X-ray component identified in IRAS 0833 is consistent with the emission from the expected number of HMXBs originated by the evolution of the starburst episode, favouring so the non-thermal nature of the hard X-ray emission, as assumed in Model 2 of Table 7.

On the other hand, the soft X-ray component associated to the emission by a thermal plasma at $kT \sim 0.62 \text{ keV}$, as in Model 2, contributes with $L_{0.4-2.4 \text{ keV}} \sim 4.2 \times 10^{40} \text{ erg s}^{-1}$. The soft X-ray emission in starburst galaxies originates from 1) the heating of the diffuse gas surrounding the stellar clusters up to temperatures of millions of Kelvin, due to the stellar winds and supernovae injecting mechanical energy into the medium, and 2) by the emission of supernova remnants (SNRs) during the adiabatic phase. The contribution by the direct emission of individual stars is negligible when compared to the previous components (Cerviño et al. 2002). Evolutionary population synthesis models CMHK02 compute the expected soft X-ray emission of a starburst after defining the physical properties of the burst, considering that a free fraction ϵ_{eff} from the mechanical energy injected



Fig. 12. Central massive stellar cluster in the starburst galaxy NGC 4214, showing the cavity formed around the massive stars. Adapted from the Hubble Heritage collection, courtesy of R. O’Connell and the WFC3 Scientific Oversight Committee.

into the medium is finally converted into soft X-ray luminosity. Typical values of $\epsilon_{\text{eff}} = 0.01 - 0.1$ are found for star-forming objects (Summers et al. 2004; Mas-Hesse et al. 2008; Mineo et al. 2012b).

The CMHK02 models for a starburst episode as defined for IRAS 0833 in Table 5 could reproduce the total observed soft X-ray luminosity $L_{0.4-2.4 \text{ keV}} \sim 1.47 \times 10^{41} \text{ erg s}^{-1}$ assuming $\epsilon_{\text{eff}} = 0.03 - 0.04$. If we remove the contribution to the soft X-ray luminosity by the non-thermal power law component, then the efficiency would be constrained to $\epsilon_{\text{eff}} = 0.01 - 0.02$. Nevertheless, since the extrapolation of the hard X-ray component to the soft X-ray range might be quite uncertain, we conclude that between 1% – 4% of the mechanical energy released by the starburst in IRAS 0833 is heating the surrounding medium, being reemitted in the form of soft X-ray photons. This value is within the usual range in starburst galaxies, as commented above. Indeed, the $L_{\text{softX}}/L_{\text{FIR}}$ ratio measured in IRAS 0833, $\log(L_{\text{softX}}/L_{\text{FIR}}) = -3.9$, is very close to the mean ratio measured by Mas-Hesse et al. (2008) on their complete sample of star-forming galaxies, $\log(L_{\text{softX}}/L_{\text{FIR}}) = -3.92$ (see Fig. 5 in Mas-Hesse et al. (2008)). We conclude therefore that the integrated soft and hard X-ray emissions of IRAS 0833 are consis-

tent with the predictions for a starburst with the properties we have derived, so that no additional sources of X-rays (e.g., a low-luminosity active galactic nucleus) have to be claimed to explain them.

4.3. Ly α emission

We show in Fig. 8 the spatial profiles of the UV continuum, Ly α and H α emissions for IRAS 0833, together with the observed values of the H α /H β and Ly α /H α ratios. The expected Ly α /H α has also been included, calculated assuming Case B recombination (Ly α /H α = 8.7, H α /H β = 2.87 (Dopita & Sutherland 2003)) and applying the dust extinction derived from the Balmer decrement. In what follows the effect of the Galactic extinction was removed before the analysis. The values of color excess, line ratios or escape fractions do not include this effect. The profiles were binned spatially, lowering the spatial resolution when needed, in order to get always a signal-to-noise ratio larger than 3. Resulting resolutions are within the range 0.1 – 0.5 arcsec pixel⁻¹. We have also plotted in the bottom panel of this figure the profile of the Ly α escape fraction, as defined by Atek et al. (2008),

$$f_{\text{esc}}^{\text{Ly}\alpha} = L_{\text{Ly}\alpha}^{\text{obs}} / L_{\text{Ly}\alpha}^{\text{int}} = L_{\text{Ly}\alpha}^{\text{obs}} / (8.7 \times L_{\text{H}\alpha}^{\text{obs}} \times 10^{0.4 \cdot E_{B-V} \cdot k_{6563}})$$

Therefore, $1 - f_{\text{esc}}^{\text{Ly}\alpha}$ represents the fraction of Ly α photons which are destroyed internally (or at least scattered out of the line of sight), either by dust absorption or by multiple interaction with the neutral gas. As we discuss below, resonant scattering redistributes the Ly α photons over large areas, so that local $f_{\text{esc}}^{\text{Ly}\alpha}$ values may differ significantly from globally integrated ones.

The spatial profiles in Fig. 8 show that in addition to the compact, central emitting blobs, a diffuse and extended Ly α component is present along the STIS slit in IRAS 0833, as discussed in Sect. 3.6. Neither of them show any clear spatial correlation with the UV continuum, Balmer decrement or H α emission whatsoever, similarly as found in Haro 2 (Oti-Flornes et al. 2012). As we concluded in Sect. 4.1, the nebular gas seems to have been pushed out by the stellar activity, creating a shell around the central, massive super-cluster SSC. This shell is being ionized by SSC and is originating most of the H α emission. Figure 8 shows that the brightest Ly α emitting regions are also located around the central cluster. Nevertheless, there is a clear spatial decoupling between the Ly α and H α profiles, as evidenced by the profile of the Ly α /H α ratio and $f_{\text{esc}}^{\text{Ly}\alpha}$ over the nuclear region, with a local maximum within the central 3'' (~1 kpc). On the other hand, the highest values of Ly α /H α ratio and $f_{\text{esc}}^{\text{Ly}\alpha}$ are detected in regions dominated by diffuse emission northward of the stellar cluster, at distances higher than 2'' (~800 pc), and in a very localized region at ~5.5'' (~2.1 kpc) to the south (Ly α S, see Figs. 8 and 13). The location of Ly α S at the outskirts of IRAS 0833 nuclear region has been marked in Fig. 2.

Oti-Flornes et al. (2012) analyzed the Ly α emission in Haro 2 and found also both compact and diffuse components, neither of them spatially coupled to UV continuum, Balmer emission or dust extinction as traced by H α /H β . However, they found that 1) diffuse Ly α emission was co-spatial to the diffuse soft X-ray emission produced by the injection of mechanical energy into the ISM by the starburst, and 2) the intensity of the diffuse Ly α emission was higher than the values predicted from H α emission assuming Case B recombination and correcting for dust extinction using the Balmer decrement. Oti-Flornes et al. (2012) argued that this diffuse emission in Haro 2 might be orig-

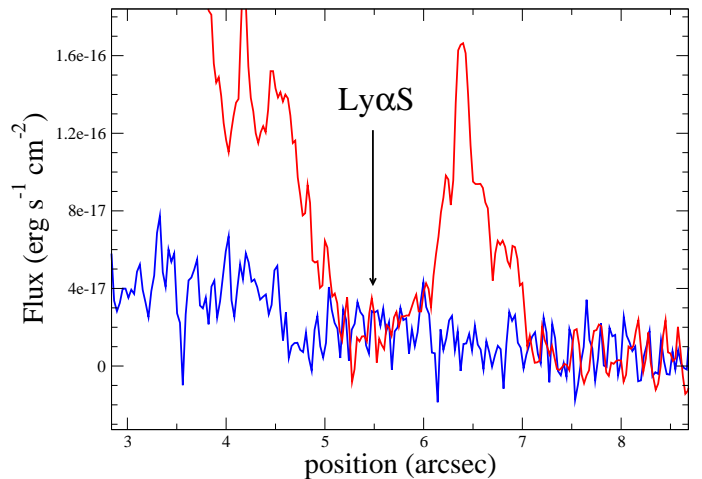


Fig. 13. Detail of the Ly α (blue) and H α (red) spatial profiles around the region at ~ 5.5'' (~2.1 kpc) south of the central SSC showing the highest value of the Ly α /H α ratio (Ly α S). The profiles have been plotted at their original resolution, 0.029 arcsec pixel⁻¹ for Ly α and 0.025 arcsec pixel⁻¹ for H α .

inated in gas ionized by the hot plasma responsible for the soft X-ray radiation, therefore not ionized by the young massive stellar clusters in the central region. Recombination in this environment would take place far from Case B conditions, causing 1) values of Ly α /H α similar to those of Case B, but with 2) large values of H α /H β , mimicking the presence of dust, and 3) values of the $L(\text{H}\alpha)/L_{0.4-2.4\text{ keV}}$ ratio much lower than when ionization is driven by massive stars. This model for the diffuse Ly α emission could explain the observed ratios in Haro 2.

But the scenario seems to be quite different in IRAS 0833. While the highest values of the Ly α /H α ratios in IRAS 0833 occur also in regions dominated by the diffuse emission, Ly α emission marginally over the values expected from Case B recombination is observed only at region Ly α S. Unfortunately, no X-ray image with enough spatial resolution is available to study 1) the co-spatiality of the diffuse soft X-ray emission and the components of Ly α , and 2) the local values of the ratio $L(\text{H}\alpha)/L_{0.4-2.4\text{ keV}}$. Thus, we can not analyze in this case whether the hot plasma could contribute significantly to the ionization of the gas in some regions, as done for Haro 2. On the other hand, the bulk of the Ly α emission comes from the region where H α is also emitted, around the central stellar cluster. The P Cyg profile of the Ly α line along the STIS slit indicates that a large fraction of the Ly α photons are being resonantly scattered out of the line of sight by the outflowing neutral gas. Relatively small variations in the properties of this outflow from one location to another, might explain why the resulting Ly α spatial profile differs from the H α one in the central 3'' area (~1 kpc). The scattering of a significant fraction of the Ly α photons explains indeed the low values of the Ly α /H α ratio along the STIS slit.

This scattering by the neutral gas surrounding SSC could transport the Ly α photons to the outer regions of IRAS 0833, leaking from the galaxy as a weak, diffuse emission halo. Fig. 4 shows in its bottom right panel the Ly α image produced by Östlin et al. (2009). While the procedure used to extract the Ly α emission in IRAS 0833 might be quite uncertain where the stellar continuum is strong (and the Ly α line shows a strong P Cyg profile), it provides a fair representation of the diffuse Ly α emission. This diffuse emission is quite homogeneous and does not follow the spatial structure of the H α emission. A good example is found in region Ly α S, as shown in Fig. 13, where Ly α /H α

becomes higher than 1 due to the local lack of $H\alpha$ photons. Eastwards of the nucleus, where the $H\alpha$ emission is less prominent, the diffuse $Ly\alpha$ remains also at a similar surface brightness than in other areas. The morphology of the $Ly\alpha$ emission supports our conclusion that the $Ly\alpha$ photons which are missing along the slit are indeed smoothly redistributed over the whole central area of IRAS 0833. Moreover, after refining the method used by Östlin et al. (2009) to remove the UV continuum from the *cont.*+ $Ly\alpha$ images, Hayes et al. (2013b) obtained $Ly\alpha$ images of the 14 star-forming galaxies of the LARS sample (Hayes et al. 2013a). Half of the sources show a conspicuous $Ly\alpha$ halo which do not present any spatial coupling to UV or $H\alpha$ emissions whatsoever. Hayes et al. (2013b) argued that resonant scattering may have redistributed the $Ly\alpha$ photons over the large areas observed. A similar situation seems to be present in IRAS 0833.

Combining the IUE $Ly\alpha$ line flux and the value of the $H\alpha$ integrated emission measured by López-Sánchez et al. (2006) we derived a globally integrated ratio $Ly\alpha/H\alpha = 0.4$ (corresponding to $f_{esc}^{Ly\alpha} \sim 0.04$). This value is ~ 10 times lower than the expected one assuming case B conditions and the average nebular extinction, $Ly\alpha/H\alpha = 4.4$. The destruction of $Ly\alpha$ photons is therefore significantly larger than the extinction extrapolated from the Balmer lines. Multiple resonant scattering of $Ly\alpha$ photons by neutral atoms increases significantly their probability of being destroyed by dust grains, yielding a much higher extinction by dust for photons around 1216 Å. As predicted by $Ly\alpha$ photons transfer models (Verhamme et al. 2006), multiple scattering can also end up shifting their energy, becoming diluted at the wings of the emission line; this effect is negligible when dust is abundant, as in the central area of IRAS 0833. This redistribution and spatial smoothing of the $Ly\alpha$ photons are responsible for the spatial decoupling between $Ly\alpha$ and $H\alpha$ emissions visible in Figs. 4 and 8. This leads to the conclusion that the star formation rate may be severely underestimated when based solely on integrated fluxes of the $Ly\alpha$ line without a proper correction of the aforementioned effects. See Fig. 2 in Hayes et al. (2011), for instance.

In any case, we do not find evidences in IRAS 0833 of any further source of $Ly\alpha$ photons like ionization by hot plasma, as it was the case in Haro 2. If present, its contribution should be negligible when compared to the ionization by massive stars. Comparison with the results on Haro 2 brings us once again to the evidence that the physics of $Ly\alpha$ photons production, transfer and destruction is extremely dependent on the conditions of each galaxy, being it difficult to find any clear correlation with the macroscopic properties of each object.

Based on the work by Tenorio-Tagle et al. (1999), Mas-Hesse et al. (2003) proposed an evolutionary picture of starbursts to try to explain the presence or lack of $Ly\alpha$ emission in star-forming galaxies, as well as the spectral features of the line. They argued that the starburst activity in IRAS 0833 has accelerated the surrounding material, forming a superbubble which expands at a velocity of $\sim 300 \text{ km s}^{-1}$ in whose interior massive stars have ionized the gas. Nebular emission lines are produced after recombination, $Ly\alpha$ among them. Due to its resonant nature, the bluest photons of the $Ly\alpha$ line are scattered by the neutral hydrogen on the shell of the superbubble, originating the P Cyg profile of the primary $Ly\alpha$ component. Furthermore, they proposed that the shock produced in the leading front may cause the shocked gas to undergo recombination. Since no dense neutral gas layers are ahead of this front, the $Ly\alpha$ photons would not be scattered and would be detected by the observer with a blueshift corresponding to the expansion velocity of

the superbubble. Mas-Hesse et al. (2003) proposed that the secondary $Ly\alpha$ component in IRAS 0833 could be produced by this mechanism. This secondary emission does not seem to be affected by neutral hydrogen scattering, which indicates that the H I column density in front of the expanding superbubble must indeed be low. This blueshifted emission is in any case weaker by an order of magnitude than the primary component, and does not contribute significantly to the integrated $Ly\alpha$ emission. According to the $Ly\alpha$ spectral profiles observed, the starburst in IRAS 0833 seems to be in the phase (d) of model by Tenorio-Tagle et al. (1999), as shown in their Fig. 8, which is characterized by a $Ly\alpha$ emission with a P Cyg profile, together with a blueshifted emission component.

On the other hand, Leitherer et al. (2013) obtained an HST/COS spectrum of IRAS 0833 which includes the $Ly\alpha$ line. They fitted its spectral profile using the radiation transfer code described by Schaerer et al. (2011), which is an improved version of the models developed by Verhamme et al. (2006). Assuming the simple geometry of an expanding spherical shell, with expansion velocity, Doppler parameter, column density and dust optical depth as free parameters, Leitherer et al. (2013) obtained a spectral profile which nicely reproduces the primary $Ly\alpha$ spectral component and predicted the presence of a secondary emission. Nevertheless, the model fails to reproduce properly the wavelength of the secondary emission peak, as well as the profile of the blue, P Cyg-like absorption wing. More detailed modeling of the $Ly\alpha$ line in IRAS 0833 would be needed to unveil the origin of this secondary $Ly\alpha$ emission.

5. Conclusions

We have carried out a multiwavelength spectral and photometric analysis of the face-on, spiral, star-forming galaxy IRAS 0833. The properties of its starburst episode and associated X-ray emission have been defined, and the morphology of the $Ly\alpha$ emission has been discussed, together with its relation to the UV continuum from the massive stars, the $H\alpha$ line and the $H\alpha/H\beta$ ratio.

- The properties of the starburst in IRAS 0833 have been defined by comparison to evolutionary population synthesis models. We conclude that a single stellar population with an age 5.5 Myr, a mass of $M \sim 1.4 \times 10^8 M_\odot$, and average stellar and nebular extinctions of $E(B-V)=0.15$ and $E(B-V)=0.06$, respectively, can account for the integrated UV, $H\alpha$ and FIR photometry, as well as for the spectral profile of the photospheric Si IV and C IV lines. The integrated UV spectrum shows the 2175 Å feature, consistent with an LMC-like extinction law.
- An underlying stellar population, some hundreds of Myrs old, dominates the IR-optical continuum in IRAS 0833, as well as the observed Ca II triplet and Mg_2 absorption lines.
- The nucleus of IRAS 0833 shows a massive cluster whose stellar continuum is barely attenuated ($E(B-V)=0.01$). We have estimated that it accounts for 20% of the observed integrated UV flux and 5% of the total mass of the starburst. The images of the nucleus show a very weak $H\alpha$ emission co-spatial to the central cluster. In fact, the synthesis models overestimate by a factor 1.5 the $H\alpha$ luminosity emitted within a central circular region of $radius = 0.5''$ ($\sim 200 \text{ pc}$). We argue that the low $H\alpha$ emission observed in this core region is due to the lack of nebular gas around the massive central cluster, which has cleaned its surroundings after pushing out the nearby gas, producing an expanding $H\alpha$ -emitting shell.

- The X-ray image does not provide any spatial information on the morphology of the emission. The starburst episode can account for the thermal soft X-ray emission detected assuming an efficiency in the conversion of mechanical energy into X-rays of $\sim 1 - 4\%$, within the typical range for starburst galaxies. The non-thermal component, which dominates the hard X-ray emission, is consistent with the number of active HMXBs expected for an evolved starburst with the properties derived for IRAS 0833.
- Two spectral Ly α components are observed. The main Ly α is detected along $16''$ (~ 6 kpc) and shows a P Cyg profile originated by resonant scattering by neutral hydrogen outflowing at ~ 300 km s $^{-1}$. The velocity structure extends all along the slit. The secondary emission is ~ 10 times weaker, extends over $6''$ (~ 2.3 kpc) and is detected over the spectral trough caused by the outflowing neutral material. All this indicates that the starburst activity has accelerated the surrounding neutral gas which no longer scatters the whole line, but only its bluest photons. In the leading front of the superbubble the gas seems to have undergone recombination, producing the secondary Ly α emission, with probably scarce neutral material ahead, so that it is detected blueshifted by ~ 300 km s $^{-1}$.
- Ly α is observed in emission along $16''$ (~ 6 kpc), without regions of total Ly α absorption. It does not show any spatial matching with the UV continuum, H α line or Balmer decrement whatsoever. Ly α photons escape mostly from two compact areas associated to, but not coincident with, the H α -emitting shell, with a size of $1''$ (~ 400 pc, north) and $1.5''$ (~ 600 pc, south). In addition, there is a diffuse Ly α component which extends northward $6''$ (~ 2.3 kpc).
- Similarly as found in other starburst galaxies, like Haro 2 (Oti-Flóranes et al. 2012), the diffuse Ly α emission shows the highest Ly α /H α ratios, as well as the highest values of the Ly α escape fraction, $f_{\text{esc}}^{\text{Ly}\alpha}$. The globally integrated Ly α /H α ratio is well below the Case B predictions (even after dereddening using the $E(B-V)_{\text{neb}}$ average value derived from the H α /H β ratio), indicating an enhanced destruction of Ly α photons with respect to the extinction extrapolated from the Balmer lines.
- We conclude that the outflowing neutral gas in front of the IRAS 0833 starburst area is resonantly scattering most of the Ly α photons, producing the observed P Cyg profile. These scattered photons are smoothly redistributed over the whole central area until either they are destroyed by interaction with dust, or escape from an extended region. Multiple scattering enhances the probability of interaction with dust, explaining why the Ly α /H α ratio values are much lower than expected for Case B conditions and the average extinction. We do not find any evidence in IRAS 0833 of any other further source of Ly α photons, like ionization by a hot plasma as proposed for Haro 2. If present, its contribution should be negligible when compared to the ionization by massive stars.
- The star formation rate in galaxies, e.g. high-redshift sources, may be severely underestimated when it is derived only from integrated fluxes of the Ly α line without a proper correction of transfer effects in the interstellar medium.

Acknowledgements. HOF and JMMH are partially funded by Spanish MINECO grants AYA2010-21887-C04-02 (*ESTALLIDOS*), AYA2011-24780/ESP and AYA2012-39362-C02-01. HOF is funded by Spanish FPI grant BES-2006-13489, CONACYT grant 129204 and a postdoctoral UNAM grant. G.Ö is a Swedish Royal Academy of Sciences research fellow supported by a grant from Knut and Alice Wallenberg foundation, and also acknowledges support from the Swedish Research Council (VR) and the Swedish National Space Board (SNSB). MH received support from the Agence Nationale de la Recherche

(ANR-09-BLAN-0234-01). HA and DK are supported by the Centre National d'Études Spatiales (CNES) and the Programme National de Cosmologie et Galaxies (PNCG). This research has made use of the Spanish Virtual Observatory (<http://svo.cab.inta-csic.es>) supported from the Spanish MICINN / MINECO through grants AyA2008-02156, AyA2011-24052. We want to acknowledge the use of the *Starburst99* models and the NASA/IPAC Extragalactic Database (NED). We are very grateful to the *ESTALLIDOS* collaboration for its scientific support. This paper was based on observations with *Hubble Space Telescope*, *XMM-Newton*, *International Ultraviolet Explorer* and *William Herschel Telescope*. We thank the anonymous referee for his comments, which helped to improve the understandability and clarity of the manuscript.

References

- Adamo, A., et al. 2010, MNRAS, 407, 870
- Arnaud, K. A. 1996, in Jacoby, G. H., Barnes, J., eds, ASP Conf. Ser. Vol. 101, Astronomical Data Analysis Software and Systems V. Astron. Soc. Pac., San Francisco, p. 17
- Atek, H., Kunth, D., Hayes, M., Östlin, G., & Mas-Hesse, J. M. 2008, A&A, 488, 491
- Calzetti, D., Armus, L., Bohlin, R. C., Kinney, A. L., Koornneef, J., & Storchi-Bergmann, T. 2000, ApJ, 533, 682
- Cannon, J. M., Skillman, E. D., Kunth, D., Leitherer, C., Mas-Hesse, J. M., Östlin, G., & Petrosian, A. 2004, ApJ, 608, 768
- Cardelli, J. A., Clayton, G. C., & Mathis, J. S. 1989, ApJ, 345, 245
- Cerviño, M., & Mas-Hesse, J. M. 1994, A&A, 284, 749
- Cerviño, M., Mas-Hesse, J. M., & Kunth, D. 1997, Revista Mexicana de Astronomía y Astrofísica Conference Series, 6, 188
- Cerviño, M., Mas-Hesse, J. M. & Kunth, D. 2002, A&A, 392, 19
- Degioia-Eastwood, K. 1992, ApJ, 397, 542
- Dickey, J. M., & Lockman, F. J. 1990, ARA&A, 28, 215
- Dopita, M. A., & Sutherland, R. S. 2003, "Astrophysics of the diffuse universe", Berlin, New York: Springer, 2003. Astronomy and astrophysics library, ISBN 3540433627
- Fitzpatrick, E. L. 1985, A&A, 299, 219
- Gadallah, K. A. K., Mutschke, H., & Jäger, C. 2011, A&A, 528, A56
- González Delgado, R. M., Leitherer, C., Heckman, T., Lowenthal, J. D., Ferguson, H. C. & Robert, C. 1998, ApJ, 495, 698
- Hayes, M., Schaerer, D., Mas-Hesse, J. M., Atek, H. & Kunth, D. 2011, ApJ, 730, 8
- Hayes, M., et al. 2013, ApJ, 765, L27
- Hayes, M., et al. 2013, arXiv:1308.6578
- Helou, G., Soifer, B. T. & Rowan-Robinson, M. 1985, ApJ, 298, L7
- Joye, W. A., & Mandel, E. 2003, in Payne, H. E., Jedrzejewski, R. I. & Hook, R. N. eds, ASP Conf. Ser. Vol. 295, Astronomical Data Analysis Software and Systems XII, p. 489
- Kalberla, P. M. W., Burton, W. B., Hartmann, D. H., Arnal, E. M., Bajaja, E., Morras, R., & Pöppel, W. G. L. 2005, A&A, 440, 775
- Kunth, D., Lequeux, J., Mas-Hesse, J. M., Terlevich, E., & Terlevich, R. 1997, Rev. Mexicana Astron. Astrofis., 6, 61
- Kunth, D., Mas-Hesse, J. M., Terlevich, E., Terlevich, R., Lequeux, J., & Fall, S. M. 1998, A&A, 334, 11
- Leitherer, C., et al. 1999, ApJS, 123, 3
- Leitherer, C., Chandar, R., Tremonty, C. A., Wofford, A. & Schaerer, D. 2013, ApJ, 772, 120
- López-Sánchez, Á. R., Esteban, C., & García-Rojas, J. 2006, A&A, 449, 997
- Maíz-Apellániz, J., Mas-Hesse, J. M., Muñoz-Tuñón, C., Vílchez, J. M., & Castañeda, H. O. 1998, A&A, 329, 409
- Mas-Hesse, J. M., Kunth, D., Tenorio-Tagle, G., Leitherer, C., Terlevich, R. J., & Terlevich, E. 2003, ApJ, 598, 858
- Mas-Hesse, J. M., Oti-Flóranes, H., & Cerviño, M. 2008, A&A, 483, 71
- Mathis, J. S. 1971, ApJ, 167, 261
- Mazzarella, J. M. & Boroson, T. A. 1993, ApJS, 85, 27
- Mewe, R., Gronenschild, E.H.B.M., & van den Oord, G.H.J., 1985, A&AS, 62, 197
- Mezger, P. G. 1978, A&A, 70,
- Mineo, S., Gilfanov, M., & Sunyaev, R. 2012, MNRAS, 419, 2095
- Mineo, S., Gilfanov, M., & Sunyaev, R. 2012, MNRAS, 426, 1870
- Östlin, G., Hayes, M., Kunth, D., Mas-Hesse, J. M., Leitherer, C., Petrosian, A., & Atek, H. 2009, AJ, 138, 923
- Oti-Flóranes, H., Mas-Hesse, J. M., Jiménez-Bailón, E., Schaerer, D., Hayes, M., Östlin, G., Atek, H., & Kunth, D. 2012, A&A, 546, A65
- Pellerin, A. & Robert, C. 1999, in Hubeny, I., Heap, S. R., & Cornett, R. H. eds, ASP Conf. Ser. Vol. 192, p. 57, Spectrophotometric Dating of Stars and Galaxies
- Petrosian, V., Silk, J., & Field, G. B. 1972, ApJ, 177, L69
- Prévot, M. L., et al. 1984, A&A, 132, 389

- Raymond, J. C. & Smith, B. W. 1977, *ApJS*, 35, 419
- Schaerer, D., & Vacca, W. D. 1998, *ApJ*, 497, 618
- Schaerer, D., Hayes, M., Verhamme, A., & Teyssier, R. 2011, *A&A*, 531, A12
- Stevens, I. R. & Strickland, D. K. 1998, *MNRAS*, 301, 215
- Summers, L. K., Stevens, I. R., & Strickland, D. K. 2001, *MNRAS*, 327, 385
- Summers, L. K., Stevens, I. R., Strickland, D. K., & Heckman, T. M. 2004, *MNRAS*, 351, 1
- Tenorio-Tagle, G., Silich, S. A., Kunth, D., Terlevich, E. & Terlevich R. 1999, *MNRAS*, 309, 332
- Verhamme, A., Schaerer, D., & Maselli, A. 2006, *A&A*, 460, 397